International Journal of Plasticity 26 (2010) 957–975

Contents lists available at ScienceDirect

International Journal of Plasticity

journal homepage: www.elsevier.com/locate/ijplas

Effect of surface/interface stress on the plastic deformation of nanoporous materials and nanocomposites

W.X. Zhang [a,b], T.J. Wang [a], X. Chen [b,c,*]

[a] MOE Key Laboratory for Strength and Vibration, Department of Engineering Mechanics, Xi'an Jiaotong University, Xi'an 710049, China
[b] Department of Earth and Environmental Engineering, Columbia University, 500 W 120th Street, New York, NY 10027, USA
[c] Department of Civil & Environmental Engineering, Hanyang University, Seoul 133-791, Republic of Korea

ARTICLE INFO

Article history:
Received 11 May 2009
Received in final revised form 1 December 2009
Available online 11 December 2009

Keywords:
Surface stress
Plasticity
Nanoporous material
Nanocomposite
Size effect

ABSTRACT

Surface and interface play an important role on the overall mechanical behaviors of nanostructured materials. We investigate the effect of surface/interface stress on the macroscopic plastic behaviors of nanoporous materials and nanocomposites, where both the surface/interface residual stress and surface/interface elasticity are taken into account. A new second-order moment nonlinear micromechanics theory is developed and then reduced to macroscopically isotropic materials. It is found that the effect of surface/interface residual stress is much more prominent than that of the surface/interface elasticity, causing strong size effect as well as asymmetric plastic deformation for tension and compression. The variation of yield strength is more prominent with smaller pore/inclusion size or higher pore/inclusion volume fraction. For a representative nanoporous aluminum, the surface effect becomes significant when the pore radius is smaller than about 50 nm. When hard inclusions are embedded in a ductile metal matrix, the interface effect and resulting size effect are much smaller than that of nanoporous materials. The results may be useful for evaluating the mechanical integrity of nanostructured materials.

1. Introduction

Nanostructured materials, such as nanoparticle composites (Balazs et al., 2006) and nanoporous materials (Russell et al., 1997), have received increasing attentions owing to their attractive physical properties and wide potential applications. The most dominant characteristics of nanocomposites (or nanoporous materials) are the ultra-small filler sizes (or pore diameters) and the ultra-high specific interface areas (or surface areas). In nanocomposites, although the addition of strong/stiff nanofillers could improve the overall strength/stiffness of the composite, however, the interface is often the "weakest link" (Frogley et al., 2003; Gan et al., 2007; Moya et al., 2007; Thostenson et al., 2001). In nanoporous materials, the ultra-large surface area is the basis for their applications in catalysis, hydrogen storage, molecular sieves, purification, energy absorption, actuation and energy harvesting, etc. (Chen et al., 2008b; Liu et al., 2008, 2009; Lu and Zhao, 2005; Morris and Wheatley, 2008). In order to fulfill their promises, the unique surface/interface effects at the nanoscale must be sufficiently understood; this is critical for the mechanical integrity and functional design of the nanostructured materials.

With the large surface/interface to volume ratio, the surface or interface energy has a significant impact on the overall mechanical properties of nanostructured materials. Many past studies focused on the effect of surface/interface on the elastic properties of nanostructured materials, such as the elastic moduli of materials with nanosized inclusions (Duan et al., 2005;

* Corresponding author. Address: Department of Earth and Environmental Engineering, Columbia University, 500 W 120th Street, New York, NY 10027, USA.
E-mail address: xichen@columbia.edu (X. Chen).

0749-6419/$ - see front matter © 2009 Elsevier Ltd. All rights reserved.
doi:10.1016/j.ijplas.2009.12.002

Yang, 2006), the diffraction of plane compressional waves around a nanosized circular hole (Wang and Wang, 2006a,b), the surface effects on the near-tip stresses for mode-I and mode-III cracks (Wang et al., 2008) and the stress concentration around nanosized voids (Ou et al., 2008; Sharma and Bhate, 2003; Wang and Wang, 2006b). In these studies, by incorporating the surface/interface effect, the elastic properties of nanostructured materials were found to be size-dependent. In addition, the presence of surface may also induce deformation instability of a thin film (Kornev and Sroloviz, 2004), as well as affecting the vibration of nanobeams (Wang and Feng, 2007), and influencing the elastic properties of nanoparticles, nanowires, and nanofilms (Cao and Chen, 2007, 2008; Dingreville et al., 2005), among others.

The interface effect (or surface effect) is also widely referred to as the interface stress (or surface stress) that consists of two parts, both arise from the distorted atomic structure near the interface (or surface): the first part is the interface (or surface) residual stress which is independent of the deformation of solids, and the second part is the interface (or surface) elasticity which contributes to the stress field related to the deformation. Duan et al. (2005) investigated the effect of interface elasticity on the effective elastic moduli of materials with nano-inclusions (with sizes below several nanometers). However, the influence of surface/interface elasticity becomes significant only when the characteristic dimension of a nano-phase is below several nanometers (Zhang and Wang, 2007; Zhang et al., 2009), and thus the effect of the surface/interface residual stress must be taken into account in most applications.[1] This can be confirmed from the bending experiments of gold nanowires with diameters 40–250 nm (Wu et al., 2005), where the size effect of Young's modulus of gold nanowire is insignificant, yet the enhancement of the yield strength is remarkable when the nanowire becomes smaller – such phenomenon cannot be explained if one only considers the surface elasticity. The prominent size effects of plastic properties also call for advances on how does the surface or interface affects the *plastic* deformation and strength of nanostructured materials; this is particularly important when nanostructured materials are used in structural components (Gleiter, 2000), MEMS or NEMS devices (Lee et al., 2006; Teh et al., 2005), or for energy absorption (Chen et al., 2006; Qiao et al., 2009), where they may need to carry significant loads over the elastic limit.

For freestanding nanowires, it was shown both experimentally and theoretically that the surface effect is prominent on the plastic behaviors. Through molecular dynamics (MD) simulations, the tensile strength of gold nanowire was found to increase with decreasing radius of the nanowires (Gall et al., 2004), and such size effect is consistent with the results of experiments (Marszalek et al., 2000; Wu et al., 2005) and theory (Zhang et al., 2008), where the surface residual stress plays a more dominant role than the surface elasticity (Zhang et al., 2008). The surface residual stress can also induce tension-compression asymmetric yield strength (Diao et al., 2004; Marszalek et al., 2000; Zhang et al., 2008). However, for the technologically important nanostructured materials (including nanocomposites and nanoporous materials), the effect of surface/interface on the overall plastic behaviors is still not well understood, and the present study aims to close such gap.

Plastic deformation, in particular the initial yielding point (i.e. the yield surface), is sensitive to the local stress (or local strain) of a heterogeneous material, which includes both the local (surface/interface) residual stress and local stress–strain relationship. Aifantis and Willis (2005) presented a variational method to investigate the influence of the interface "energy" on the overall yield strength of composites. However, the interface stress was neglected and the stress across the interface was continuous, and the interface "energy" term in their work could only influence the high-order stress. Based on the energy average of the local deformation field, the second-order moment micromechanics approach (Hu, 1996; Qiu and Weng, 1995) could effectively capture these local heterogeneous properties. Other researches have developed a different version of the second-order moment micromechanics theory based on rigorous mathematical variational principles (Ponte Castañeda, 1991; Suquet, 1993); in a follow-up work (Hu, 1996; Suquet, 1995), it was shown that these two second-order moment approaches were mathematically linked. There were few attempts of incorporating the surface/interface elasticity into such micromechanics approach (Zhang and Wang, 2007), and the influence of interface elasticity on the overall plastic behaviors of micropolar composites was estimated (Chen et al., 2008a). In those studies, the surface/interface residual stress was neglected. However, as we have pointed out, the surface/interface residual stress cannot be neglected. Indeed, plastic deformation is determined by the stress state and thus it is significantly affected by the surface/interface residual stress. Ou et al. (2008) found that the surface residual stress strongly affects the elastic stress concentration factor around a nano-sized spheroidal cavity. Thus, one could suspect that the surface/interface residual stress must have a profound influence on the plastic deformation of the nanostructured material.

The present paper extends the second-order theory to systematically explore the influences of surface/interface residual stress *and* surface/interface elasticity on the elastoplastic properties of nanostructured materials.[2] Within the context of continuum theory, the plastic deformation in the matrix should be regarded as a statistical average. In other words, although the plastic deformation around a nano-inclusion is discrete, the statistical average in all sample space is continuous. Such a continuum plasticity theory to be developed in this paper is more efficient (than discrete dislocation plasticity) of obtaining the macroscopic mechanical properties, and the continuum theory could yield good agreements with discrete dislocation plasticity (Needleman and Van der Giessen, 2001a).

The nonlinear micromechanics model is based on the secant moduli of nonlinear matrix and field fluctuation method, and through representative numerical examples of nanoporous aluminum and SiC nanoparticle reinforced Al matrix, we demonstrate that the effect of surface/interface residual stress is prominent on the shifting of yield surface and causing the size

[1] The mechanical properties of nonlinear materials are coupled with the deformation field, and thus the surface/interface residual stress can influence the deformation field or stress field.

[2] To highlight the effect of surface/interface stress, we do not take into account the strain gradient effect in this study.

effect, and it also induces tension-compression asymmetry. The results may be useful for evaluating the mechanical integrity and reliability of nanoporous materials and nanocomposites.

2. Model and methods

2.1. Surface/interface stress

Since nanoporous materials may be regarded as a special subset of nanocomposite where the inclusions are voids, in what follows, the surface effect/energy/stress of nanoporous materials is also referred to as the interface effect/energy/stress. The interface stress is related to the interface energy (Cammarata, 1994; Shuttleworth, 1950):

$$\boldsymbol{\tau} = \gamma \mathbf{I}^{(2)} + \frac{\partial \gamma}{\partial \boldsymbol{\varepsilon}^i} \tag{1}$$

where γ is the excess free energy per unit interface area (Nix and Gao, 1998; Vermaak et al., 1968), $\mathbf{I}^{(2)}$ is the second-order unit tensor in two-dimensional space, and $\boldsymbol{\varepsilon}^i$ is the interface strain tensor. In this paper, the bold letter represents a tensor or vector, and the superscript i denotes the interface property. In essence, γ can be affected by the deformation of the interface (Cammarata, 1994). To simplify the analysis, here we assume that $\boldsymbol{\tau}$ is invariant during plastic deformation. According to the model introduced by Gurtin and Murdoch (1975), the interface stress is the summation of the interface residual stress and interface elasticity:

$$\boldsymbol{\tau} = \boldsymbol{\tau}_0 + \mathbf{s}^i : \boldsymbol{\varepsilon}^i \tag{2}$$

where $\boldsymbol{\tau}_0$ is the interface residual stress and $\mathbf{s}^i$ is the interface stiffness tensor. Physically, the interface residual stress and interface elasticity are related to the crystal surface orientation and they are intrinsic properties of the interface; in general, both $\boldsymbol{\tau}_0$ and $\mathbf{s}^i$ can be inhomogeneous and anisotropic.

In the special case where the interface property is isotropic, the interface constitutive equation is the following:

$$\boldsymbol{\tau} = \tau_0 \mathbf{I}^{(2)} + 2\mu^i \boldsymbol{\varepsilon}^i + \lambda^i (\mathrm{tr}\, \boldsymbol{\varepsilon}^i) \mathbf{I}^{(2)} \tag{3}$$

where μ^i and λ^i are the shear modulus and Lame's constant of the interface, respectively. If the interface properties are homogeneous, the values of τ_0, μ^i, and λ^i are the same everywhere on the interface.

Although the interface residual stress does not influence the effective Young's modulus of nano-materials, its effect on the plastic behaviors is significant (much more than the interface elasticity) (Zhang et al., 2008). Since the surface deformation is usually small before plastic deformation occurs, the second term on the right side of Eq. (2) is relatively small.

For linear elastic "bulk" materials, the equilibrium and constitutive equations are:

$$\nabla \cdot \boldsymbol{\sigma}_k = 0 \tag{4}$$

$$\boldsymbol{\sigma}_k = \mathbf{s}_k : \boldsymbol{\varepsilon}_k \tag{5}$$

where ∇g is the divergence operator, $\boldsymbol{\sigma}_k$ is the stress tensor, $\boldsymbol{\varepsilon}_k$ is the strain tensor, and $\mathbf{s}_k$ is the stiffness tensor. In this paper, when the subscript k takes 0 or 1, it represents the matrix property or inclusion property, respectively. Under small deformation, the strain is defined as

$$\boldsymbol{\varepsilon}_k = \frac{1}{2}(\nabla \otimes \mathbf{u}_k + \mathbf{u}_k \otimes \nabla) \tag{6}$$

where $\mathbf{u}_k$ is the displacement and ∇ is the gradient operator. In the special case where the material is isotropic, the constitutive relationship is

$$\boldsymbol{\sigma}_k = \lambda_k (\mathrm{tr}\, \boldsymbol{\varepsilon}_k) \mathbf{I}^{(3)} + 2\mu_k \boldsymbol{\varepsilon}_k \tag{7}$$

where λ_k and μ_k are the Lame's constant and shear modulus of the material (phase), respectively, and $\mathbf{I}^{(3)}$ is the second-order unit tensor in three-dimensional space.

The interface stress and the stress within each phase satisfy the generalized Young–Laplace equations (Sharma and Bhate, 2003):

$$\begin{aligned} \mathbf{n} \cdot [\boldsymbol{\sigma}] \cdot \mathbf{n} &= -\boldsymbol{\tau} : \mathbf{b} \\ \mathbf{P} \cdot [\boldsymbol{\sigma}] \cdot \mathbf{n} &= -\nabla^i \cdot \boldsymbol{\tau} \end{aligned} \tag{8}$$

where $\mathbf{n}$ is the unit normal vector on the interface whose positive direction is from the void (inclusion) to the matrix, $\mathbf{P} = \mathbf{I}^{(3)} - \mathbf{n} \otimes \mathbf{n}$, $\nabla^i \cdot \boldsymbol{\tau}$ is the interface divergence of the interface stress $\boldsymbol{\tau}$, $[\boldsymbol{\sigma}]$ is the stress jump across the interface from the inclusion to the matrix (due to the existence of interface stress), and $\mathbf{b}$ is the curvature tensor (for the details of the components of $\mathbf{b}$, please refer to the work of Huang and Wang (2006)).

2.2. Representative volume element (RVE)

The three-dimensional RVE includes a sufficiently large number of nano-sized inclusions (Fig. 1), where the inclusion shape and distribution can be arbitrary in the general approach. When the sizes of inclusions are different, they must be taken as different inclusions since the influences of their interface stresses are different. For convenience, we first define the terminologies for three configurations of RVE: the *reference* configuration, the *initial* configuration, and the *current* configuration. In the reference configuration, the interface residual stress is assumed to be zero – at this stage there is no stress in the material. Next, we add $\boldsymbol{\tau}_0$ on the interface and subsequently, the inclusion, interface, and matrix will deform until a new equilibrium is reached, which is referred to as the initial configuration (in absence of any external load). When an external load $\mathbf{F}$ is applied, the RVE will further deform to a new equilibrium configuration, which is the current configuration. Note that during a real experiment, only the initial and current configurations may be experienced.

In this paper, the displacement $\mathbf{u}_k$ and interface residual stress $\boldsymbol{\tau}_0$ are defined with respect to the reference configuration. $\boldsymbol{\tau}_0$ is independent of deformation and it depends only on the crystal orientation for a given material. While these are "local" quantities, for the RVE, the macroscopic stress $\bar{\boldsymbol{\sigma}}$ and strain $\bar{\boldsymbol{\varepsilon}}$ are defined as follows (Nemat-Nasser and Hori, 1993):

$$\begin{aligned}\bar{\boldsymbol{\sigma}} &= \tfrac{1}{V}\int_{S_{\text{out}}} \mathbf{X}\otimes\mathbf{F}\,dS \\ \bar{\boldsymbol{\varepsilon}} &= \tfrac{1}{V}\int_{S_{\text{out}}} \tfrac{1}{2}(\mathbf{n}\otimes\mathbf{u}+\mathbf{u}\otimes\mathbf{n})\,dS\end{aligned} \tag{9}$$

where $\mathbf{X}$ is the position vector of the outer boundary, $\mathbf{n}$ the outer unit normal vector of RVE, and $\mathbf{u}$ the displacement of the boundary. These definitions are with respect to the reference configuration. S_{out} is the outer surface of the RVE; correspondingly, the "inner" surface, or the interface, is denoted as S_{in}.

2.3. Principle of virtual work (PVW) and Hill's lemma of RVE

Denote the volume of matrix as V_0 and the volume of inclusion as V_1. First, the PVW can be applied to each individual phase separately. For phase 0 (matrix),

$$\int_{S_{\text{out}}} \mathbf{F}\cdot\mathbf{u}\,dS + \int_{S_{\text{in}}} \mathbf{F}^0_{\text{in}}\cdot\mathbf{u}\,dS = \int_{V_0} \boldsymbol{\sigma}_0 : \boldsymbol{\varepsilon}_0\,dV \tag{10}$$

where $\mathbf{F}^0_{\text{in}}$ is the traction force at the interface whose positive direction is from the matrix to the inclusion. In phase 1 (inclusion) we have

$$\int_{S_{\text{in}}} \mathbf{F}^1_{\text{in}}\cdot\mathbf{u}\,dS = \int_{V_1} \boldsymbol{\sigma}_1 : \boldsymbol{\varepsilon}_1\,dV \tag{11}$$

where $\mathbf{F}^1_{\text{in}}$ is the traction force of the inclusion whose positive direction is from the inclusion to the matrix. Add these two equations and note that $-[\boldsymbol{\sigma}]\cdot\mathbf{n} = \mathbf{F}^0_{\text{in}} + \mathbf{F}^1_{\text{in}}$ (where $\mathbf{n}$ is the normal unit vector of the interface and its positive direction is toward the matrix.):

$$\int_{S_{\text{out}}} \mathbf{F}\cdot\mathbf{u}\,dS - \int_{S_{\text{in}}} [\boldsymbol{\sigma}]\cdot\mathbf{n}\cdot\mathbf{u}\,dS = \int_{V} \boldsymbol{\sigma} : \boldsymbol{\varepsilon}\,dV \tag{12}$$

The derived PVW of the RVE is valid for any inclusion size, distribution, and material properties. By using the PVW, the Hill's lemma for RVE with interface stress can be derived as the following (which is the foundation of the present paper, see Appendix A for details):

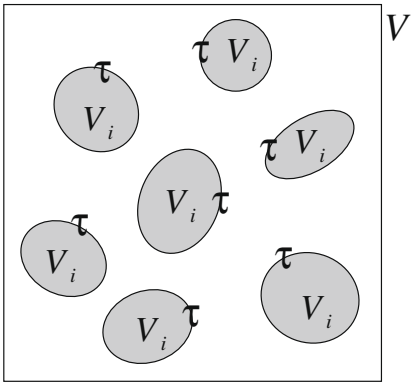

Fig. 1. Schematic of the general RVE model whose volume is V. V_i is the inclusion volume and interface/surface stress is $\boldsymbol{\tau}$. In the general theory developed in this paper, the material/interface properties can be inhomogeneous and anisotropic, and the inclusion shape/size can be different. In Section 2.5 and later the solutions are specified for a macroscopically isotropic RVE, where the inclusions are spherical with same radius R, and they distribute homogeneously and isotropically in the matrix.

$$\bar{\boldsymbol{\sigma}} : \bar{\boldsymbol{\varepsilon}} - \frac{f_i}{V_i} \int_{\partial V_i} \boldsymbol{\tau} : \boldsymbol{\varepsilon}^i \, ds = \langle \boldsymbol{\sigma} : \boldsymbol{\varepsilon} \rangle \tag{13}$$

where V_i is the volume enclosed by the interface and $\partial V_i = S_{in}$; note that $V_i = V_1$ if there is only one kind of inclusion, yet we denote it as V_i in Sections 2.3 and 2.4 because in the present general approach, multiple inclusions are allowed and their sizes may vary. f_i is the volume fraction of inclusion and for any variable Φ, $\langle \Phi \rangle \equiv \frac{1}{V} \int_V \Phi \, dV$ over the RVE. It should be pointed out that the stress and strain in Eq. (13) can be arbitrary as long as they satisfy equilibrium (Eqs. (4) and (8)) with continuous displacement (Eq. (6)).

The deformation field of the inclusions is contributed by both the external load and the interface residual stress. For linear elastic material, by utilizing the superposition principle, the deformation field can be decomposed into the summation of two parts: the one caused by the external load and that caused by the interface residual stress. In other words, $\bar{\boldsymbol{\varepsilon}} = \bar{\boldsymbol{\varepsilon}}_\sigma + \bar{\boldsymbol{\varepsilon}}_\tau$ and $\boldsymbol{\varepsilon}^i = \boldsymbol{\varepsilon}^i_\sigma + \boldsymbol{\varepsilon}^i_\tau$. Here, $\bar{\boldsymbol{\varepsilon}}_\sigma$ is the macroscopic strain generated by the external load $\bar{\boldsymbol{\sigma}}$, and $\bar{\boldsymbol{\varepsilon}}_\tau$ is the macroscopic strain due to the interface residual stress $\boldsymbol{\tau}_0$. $\boldsymbol{\varepsilon}^i_\sigma$ and $\boldsymbol{\varepsilon}^i_\tau$ are the interface strain caused by the external load and the interface residual stress, respectively. Using Eq. (2), Eq. (13) becomes

$$\bar{\boldsymbol{\sigma}} : \bar{\boldsymbol{\varepsilon}}_\sigma + \bar{\boldsymbol{\sigma}} : \bar{\boldsymbol{\varepsilon}}_\tau - \frac{f_i}{V_i} \int_{\partial V_i} \left(\boldsymbol{\tau}_0 : \boldsymbol{\varepsilon}^i_\sigma + \boldsymbol{\tau}_0 : \boldsymbol{\varepsilon}^i_\tau + \boldsymbol{\varepsilon}^i : \mathbf{s}^i : \boldsymbol{\varepsilon}^i \right) ds = \langle \boldsymbol{\sigma} : \boldsymbol{\varepsilon} \rangle \tag{14}$$

Recall the reciprocal theorem

$$\bar{\boldsymbol{\sigma}} : \bar{\boldsymbol{\varepsilon}}_\tau = -\frac{f_i}{V_i} \int_{\partial V_i} \boldsymbol{\tau}_0 : \boldsymbol{\varepsilon}^i_\sigma \, ds \tag{15}$$

Eq. (14) can be simplified as

$$\bar{\boldsymbol{\sigma}} : \bar{\boldsymbol{\varepsilon}}_\sigma + 2\bar{\boldsymbol{\sigma}} : \bar{\boldsymbol{\varepsilon}}_\tau - \frac{f_i}{V_i} \int_{\partial V_i} \left(\boldsymbol{\tau}_0 : \boldsymbol{\varepsilon}^i_\tau + \boldsymbol{\varepsilon}^i : \mathbf{s}^i : \boldsymbol{\varepsilon}^i \right) ds = \langle \boldsymbol{\sigma} : \boldsymbol{\varepsilon} \rangle \tag{16}$$

The effective compliance tensor of the RVE (corresponding to the external load) is $\overline{\mathbf{C}}$, i.e. $\bar{\boldsymbol{\varepsilon}}_\sigma = \overline{\mathbf{C}} : \bar{\sigma}$. The residual stress at any point in the interface is also constrained by the entire RVE, from which a compliance tensor $\overline{\mathbf{C}}_\tau$ is defined as $\bar{\boldsymbol{\varepsilon}}_\tau = \int_{\partial V_i} \overline{\mathbf{C}}_\tau : \boldsymbol{\tau}_0 \, ds$; note that for a general interface between two anisotropic solids, $\overline{\mathbf{C}}_\tau$ may be inhomogeneous on the interface. The overall effect of $\boldsymbol{\tau}_0$ leads to the macroscopic strain $\bar{\boldsymbol{\varepsilon}}_\tau$. Also denote $\mathbf{C}_\tau$ as the compliance tensor of interface under the constraint of RVE according to $\boldsymbol{\varepsilon}^i_\tau = \mathbf{C}_\tau : \boldsymbol{\tau}_0$. Eq. (14) can now be rewritten as

$$\bar{\boldsymbol{\sigma}} : \overline{C} : \bar{\sigma} + 2\bar{\boldsymbol{\sigma}} : \int_{\partial V_i} \overline{\mathbf{C}}_\tau : \boldsymbol{\tau}_0 \, ds - \frac{f_i}{V_i} \int_{\partial V_i} \left(\boldsymbol{\tau}_0 : \mathbf{C}_\tau : \boldsymbol{\tau}_0 + \boldsymbol{\tau}^i : \mathbf{c}^i : \boldsymbol{\tau}^i \right) ds = \langle \boldsymbol{\sigma} : \mathbf{c} : \boldsymbol{\sigma} \rangle \tag{17}$$

where $\boldsymbol{\tau}^i = \mathbf{s}^i : \boldsymbol{\varepsilon}^i$ is the interface stress caused by the interface elasticity, and $\boldsymbol{\varepsilon}^i = \mathbf{c}^i : \boldsymbol{\tau}^i$. And the material "local" compliance tensor $\mathbf{c} = \mathbf{s}^{-1}$, with $\mathbf{c} = \mathbf{c}_0$ for matrix and $\mathbf{c} = \mathbf{c}_1$ for inclusion, that satisfy $\boldsymbol{\varepsilon}_k = \mathbf{c}_k : \boldsymbol{\sigma}_k$ ($k = 0,1$).

2.4. Field fluctuation method

Several micromechanics methods are available to obtain the macroscopic properties of linear elastic heterogeneous materials, e.g. the Mori–Tanaka method (Chen et al., 1992; Kitazono et al., 2003), self-consistent method (Hill, 1965), Hashin-Strikman variational method (Hashin and Shtrikman, 1963; Hashin, 1983), among others (Li and Wang, 2005). Such approach can be extended to nonlinear heterogeneous materials, whose moduli are related to the deformation state: at a given strain, the nonlinear material may be characterized by a *linear comparison material* whose properties are described by the instantaneous secant moduli of the nonlinear material, and the secant moduli are strain dependent. Therefore, one could focus on the macroscopic properties of the heterogeneous linear comparison material, which has the same configuration as the nonlinear material at every deformation stage and thus provides a good estimation (Hu, 1996; Qiu and Weng, 1992, 1993, 1995). In this approach, one must first obtain the stress or strain so as to derive the instantaneous secant moduli. Since the stress field is heterogeneous in a composite material, in principle, the secant moduli are also heterogeneous and thus it is impossible to obtain the exact local stress/strain solutions of a heterogeneous material. In order to simplify the analysis, we adopt the widely used assumption (Hu, 1996; Ponte Castañeda, 1991, 1996; Ponte Castañeda and Suquet, 1997; Qiu and Weng, 1992, 1993, 1995; Tandon and Weng, 1988) and assume that the secant modulus of any nonlinear phase (e.g. within the matrix) is uniform.[3] In this paper, we assume that the matrix material is nonlinear (i.e. plastic deformation occurs only in the matrix) whereas the inclusion in a nanocomposite material is elastic, which is a reasonable assumption since the nanoparticle fillers are usually very hard; the inclusion is void in a nanoporous material. Of course, the overall behavior of the composite is nonlinear.

[3] Note that the stress and strain are still heterogeneous within the present micromechanics approach, but instead we assume that the secant modulus of a nonlinear phase (e.g. the metal matrix) is a function of an averaged equivalent stress of this phase, and thus the secant modulus is uniform within this phase, see Section 2.5 for details.

The local stress can be obtained by the following field fluctuation procedure. Under the constant stress boundary condition and constant interface residual stress, let the local compliance tensor $\mathbf{c}$ to undergo a small variation $\delta\mathbf{c}$; this will lead to stress perturbations $\delta\boldsymbol{\sigma}$ and $\delta\boldsymbol{\tau}$. The corresponding variations of $\overline{\mathbf{C}}, \overline{\mathbf{C}}_\tau$, and $\mathbf{C}_\tau$ are $\delta\overline{\mathbf{C}}, \delta\overline{\mathbf{C}}_\tau$ and $\delta\mathbf{C}_\tau$, respectively:

$$\bar{\boldsymbol{\sigma}} : \delta\overline{\mathbf{C}} : \bar{\boldsymbol{\sigma}} + 2\bar{\boldsymbol{\sigma}} : \int_{\partial V_i} \delta\overline{\mathbf{C}}_\tau : \boldsymbol{\tau}_0 \, ds - \frac{f_i}{V_i} \int_{\partial V_i} \left(\boldsymbol{\tau}_0 : \delta\mathbf{C}_\tau : \boldsymbol{\tau}_0 + 2\delta\boldsymbol{\tau}^i : \mathbf{c}^i : \boldsymbol{\tau}^i\right) ds = \langle \boldsymbol{\sigma} : \delta\mathbf{c} : \boldsymbol{\sigma} \rangle + 2\langle \delta\boldsymbol{\sigma} : \mathbf{c} : \boldsymbol{\sigma} \rangle \tag{18}$$

Using the Hill's condition, Eq. (13), we have

$$-\frac{f_i}{V_i} \int_{\partial V_i} 2\delta\boldsymbol{\tau}^i : \mathbf{c}^i : \boldsymbol{\tau}^i \, ds = 2\langle \delta\boldsymbol{\sigma} : \mathbf{c} : \boldsymbol{\sigma} \rangle \tag{19}$$

Thus,

$$\bar{\boldsymbol{\sigma}} : \delta\overline{\mathbf{C}} : \bar{\boldsymbol{\sigma}} + 2\bar{\boldsymbol{\sigma}} : \int_{\partial V_i} \delta\overline{\mathbf{C}}_\tau : \boldsymbol{\tau}_0 \, ds - \frac{f_i}{V_i} \int_{\partial V_i} \boldsymbol{\tau}_0 : \delta\mathbf{C}_\tau : \boldsymbol{\tau}_0 \, ds = \langle \boldsymbol{\sigma} : \delta\mathbf{c} : \boldsymbol{\sigma} \rangle \tag{20}$$

Eq. (20) shows that the fluctuation of local compliance leads the perturbation of macroscopic compliance. Utilizing Eq. (20) one can obtain the relationship between the second moment of local stress and the macroscopic stress under the aforementioned assumption of uniform secant moduli in the nonlinear phase (matrix in this paper).

When the interface residual stress is homogeneous and isotropic, the formulation can be further simplified. Assuming $\boldsymbol{\tau}_0 = \tau_0 \mathbf{I}^{(2)}$ holds everywhere on the interface, Eq. (17) can be further simplified as

$$\bar{\boldsymbol{\sigma}} : \overline{\mathbf{C}} : \bar{\sigma} + 2\tau_0 \bar{\boldsymbol{\sigma}} : \int_{\partial V_i} \overline{\mathbf{C}}_\tau : \mathbf{I}^{(2)} ds - \frac{f_i \tau_0^2}{V_i} \int_{\partial V_i} \mathbf{I}^{(2)} : \mathbf{C}_\tau : \mathbf{I}^{(2)} \, ds - \frac{f_i}{V_i} \int_{\partial V_i} \boldsymbol{\tau}^i : \mathbf{c}^i : \boldsymbol{\tau}^i \, ds = \langle \boldsymbol{\sigma} : \mathbf{c} : \boldsymbol{\sigma} \rangle \tag{21}$$

By letting $\overline{\mathbf{B}} = \int_{\partial V_i} \overline{\mathbf{C}}_\tau : \mathbf{I}^{(2)} ds$ and $\overline{D} = \int_{\partial V_i} \mathbf{I}^{(2)} : \mathbf{C}_\tau : \mathbf{I}^{(2)} ds$,

$$\bar{\boldsymbol{\sigma}} : \overline{\mathbf{C}} : \bar{\boldsymbol{\sigma}} + 2\tau_0 \bar{\boldsymbol{\sigma}} : \overline{\mathbf{B}} - \frac{f_i \tau_0^2}{V_i} \overline{D} - \frac{f_i}{V_i} \int_{\partial V_i} \boldsymbol{\tau}^i : \mathbf{c}^i : \boldsymbol{\tau}^i \, ds = \langle \boldsymbol{\sigma} : \mathbf{c} : \boldsymbol{\sigma} \rangle \tag{22}$$

It should be noted that both $\overline{\mathbf{B}}$ and $\overline{D}$ are compliance-like quantities, where $\overline{\mathbf{B}}$ is the compliance tensor corresponding to the macroscopic deformation of RVE caused by an unit interface stress, and $\overline{D}$ is the microscopic compliance corresponding to the local interface strain induced by an unit interface stress. Note that the interface is constrained by the whole RVE as well, and thus $\overline{D}$ is related to the whole RVE.

With the field fluctuation method the following relationship is obtained:

$$\bar{\boldsymbol{\sigma}} : \delta\overline{\mathbf{C}} : \bar{\sigma} + 2\tau_0 \bar{\boldsymbol{\sigma}} : \delta\overline{\mathbf{B}} - \frac{f_i \tau_0^2}{V_i} \delta\overline{D} = \langle \boldsymbol{\sigma} : \delta\mathbf{c} : \boldsymbol{\sigma} \rangle \tag{23}$$

The generic formulation presented above is valid as long as the interface residual stress is isotropic and homogeneous; all other general material/interface properties can be inhomogeneous and anisotropic.

2.5. Solution for isotropic RVE

The microstructure of nanocomposites and nanoporous materials can be complex and affected by many factors (Banhart, 2001; Gleiter, 2000); it may be impossible to capture all the details of an irregular microstructure. The main emphasis of this paper is to present a micromechanics approach to investigate the interface stress – macroscopic property relationship. In what follows, we apply the developed theory to a composite whose matrix is elastoplastic and isotropic, and the inclusion is linear elastic and isotropic. The interface properties are also assumed to be uniform. Therefore, the local compliance moduli $\mathbf{c}^i$ and $\mathbf{c}$ are taken to be homogeneous and isotropic. We assume all inclusions are spherical and of same radius R, and they are distributed homogeneously and randomly in the matrix; in this case the interface residual stress only induces a macroscopic volumetric deformation, thus, $\overline{\mathbf{B}} = \overline{B}\mathbf{I}^{(3)} = \bar{\varepsilon}_\tau / \tau_0, \overline{D} = \frac{1}{\tau_0} \int_{\partial V_i} tr(\boldsymbol{\varepsilon}^i) ds$, and the compliance moduli $\overline{\mathbf{C}}_\tau$, $\mathbf{C}_\tau$, $\overline{\mathbf{C}}$, are homogeneous and isotropic.

With these simplifications, the macroscopic moduli $\overline{\mathbf{B}}$ and $\overline{D}$ in Eq. (23) can be derived in closed form by the Hashin sphere model (Hashin and Shtrikman, 1963):

$$\overline{\mathbf{B}} = \overline{B}\mathbf{I}^{(3)} = \frac{2f_1(4\mu_0 + 3k_0)\mathbf{I}^{(3)}}{R\left[\mu_0(f_1 - 1)k_0 - \left(\frac{4}{3}f_1\mu_0 + k_0\right)\left(\frac{1}{2}\mu_0 k_s^r - \frac{3}{4}k_1\right)\right]} \tag{24}$$

$$\overline{D} = \frac{(4\mu_0 f_1 + 3k_0)}{R^2\left[\mu_0(f_1 - 1)k_0 - \left(\frac{4}{3}f_1\mu_0 + k_0\right)\left(\frac{1}{2}\mu_0 k_s^r - \frac{3}{4}k_1\right)\right]} \tag{25}$$

The detailed derivation is given in Appendix B. The bulk modulus and shear modulus of the matrix are k_0 and μ_0, respectively, and that of the inclusion are k_1 and μ_1. $k_s^r = k^i/(R\mu_0)$, where the bulk modulus of the interface is $k^i = 2(\mu^i + \lambda^i)$ (see Eq. (3)). f_1 is the volume fraction of the spherical nano-inclusion with radius R.

The constitutive equation of the isotropic RVE is

$$\bar{\boldsymbol{\sigma}} = \left(\overline{K} - \frac{2}{3}\overline{G}\right)(\mathrm{tr}\,\bar{\boldsymbol{\varepsilon}})\mathbf{I}^{(3)} + 2\overline{G}\bar{\boldsymbol{\varepsilon}} \tag{26}$$

where $\overline{K}$ and $\overline{G}$ are the bulk modulus and shear modulus of RVE, which should be regarded as the secant moduli for the nonlinear material. $\overline{K}$ and $\overline{G}$ can be derived by several methods, such as the self-consistent method (Christensen and Lo, 1979) or Mori–Tanaka method (Tandon and Weng, 1988). Following the work of Duan et al. (2005), they can be obtained as:

$$\overline{K} = \frac{3k_1(3k_0 + 4f_1\mu_0) + 2\mu_0[4f_1\mu_0 k_s^r + 3k_0(2 - 2f_1) + k_s^r]}{3[3(1 - f_1)k_1 + 3f_1k_0 + 2\mu_0(2 + k_s^r - f_1k_s^r)]} \tag{27}$$

$$\overline{G} = \frac{\mu_0[5 - 8f_1\xi_3(7 - 5v_0)]}{5 - f_1(5 - 84\xi_1 - 20\xi_2)} \tag{28}$$

where

$$\xi_1 = \frac{15(1 - v_0)(k_s^r + 2\mu_s^r)}{4H} \tag{29}$$

$$\xi_2 = \frac{-15(1 - v_0)}{4H}[\eta_1(7 + 5v_1) - 8v_1(5 + 3k_s^r + \mu_s^r) + 7(4 + 3k_s^r + 2\mu_s^r)] \tag{30}$$

$$\xi_3 = \frac{5}{16H}\{2\eta_1^2(7 + 5v_1) - 4(7 - 10v_1)(2 + k_s^r)(1 - \mu_s^r) + \eta_1[7(6 + 5k_s^r + 4\mu_s^r) - v_1(90 + 47k_s^r + 4\mu_s^r)]\} \tag{31}$$

$$\begin{aligned} H = {} & -2\eta_1^2(7 + 5v_1)(4 - 5v_2) + 7\eta_1\left[-39 - 20k_s^r - 16\mu_s^r + 5v_2(9 + 5k_s^r + 4\mu_s^r)\right] \\ & + \eta_1 v_1\left[285 + 188k_s^r + 16\mu_s^r - 5v_2(75 + 47\kappa_s^r + 4\mu_s^r)\right] + 4(7 - 10v_1)\left\{-7 - 11\mu_s^r - k_s^r(5 + 4\mu_s^r)\right. \\ & \left. + v_2\left[5 + 13\mu_s^r + k_s^r(4 + 5\mu_s^r)\right]\right\} \end{aligned} \tag{32}$$

with $\mu_s^r = \mu^i/(R\mu_0)$ and $\eta_1 = \mu_1/\mu_0$.

The macroscopic stress of the isotropic RVE as well as the local stress can be decomposed into deviatoric and spherical parts:

$$\bar{\boldsymbol{\sigma}} = \bar{\boldsymbol{\sigma}}' + \bar{\sigma}_m\mathbf{I}^{(3)} \tag{33}$$

$$\boldsymbol{\sigma} = \boldsymbol{\sigma}' + \sigma_m\mathbf{I}^{(3)} \tag{34}$$

where $\bar{\boldsymbol{\sigma}}'$ is the macroscopic stress deviator and $\bar{\sigma}_m = \frac{1}{3}tr\bar{\boldsymbol{\sigma}}$, $\boldsymbol{\sigma}'$ is the local stress deviator and $\sigma_m = \frac{1}{3}tr\boldsymbol{\sigma}$. The deformation of RVE can also be resolved into two parts, i.e. the volume change and the shape variation. When the shear modulus of the matrix, μ_0, undergoes a small variation, the relationship between the second moment of local deviatoric stress and the macroscopic stress can be established:

$$(\bar{\boldsymbol{\sigma}}' : \bar{\boldsymbol{\sigma}}')\delta\left(\frac{1}{2\overline{G}}\right) + \bar{\sigma}_m^2\delta\left(\frac{1}{\overline{K}}\right) + 2\tau_0\bar{\boldsymbol{\sigma}} : \delta\overline{\mathbf{B}} - \frac{f_1\tau_0^2}{V_1}\delta\overline{D} = (1 - f_1)\delta\left(\frac{1}{2\mu_0}\right)\langle\boldsymbol{\sigma}' : \boldsymbol{\sigma}'\rangle_{V_0} \tag{35}$$

where V_0 is the volume of matrix and V_1 is the volume of inclusion. We assume that the matrix obeys the Mises yield criterion and follows the isotropic harden rule. If we know the form of the macroscopic compliance in advance, which is a function of the compliance of the constituent phases, we can change the variation form to a differential form so as to correlate the local stress with macroscopic stress. With $\sigma_e^2 = \frac{3}{2}\boldsymbol{\sigma}' : \boldsymbol{\sigma}'$ and $\bar{\sigma}_e^2 = \frac{3}{2}\bar{\boldsymbol{\sigma}}' : \bar{\boldsymbol{\sigma}}'$:

$$\bar{\sigma}_e^2\left(\frac{\mu_0}{\overline{G}}\right)^2\frac{\partial\overline{G}}{\partial\mu_0} + 3\bar{\sigma}_m^2\left(\frac{\mu_0}{\overline{K}}\right)^2\frac{\partial\overline{K}}{\partial\mu_0} - 18\bar{\sigma}_m\tau_0\mu_0^2\frac{\partial\overline{B}}{\partial\mu_0} + 3\frac{f_1}{V_1}\tau_0^2\mu_0^2\frac{\partial\overline{D}}{\partial\mu_0} = (1 - f_1)\langle\sigma_e^2\rangle_{V_0} = (1 - f_1)\bar{\sigma}_{e0}^2 \tag{36}$$

where $\bar{\sigma}_{e0}^2 = \langle\sigma_e^2\rangle_{V_0}$. Eq. (36) establishes the relationship between the macroscopic stress ($\bar{\sigma}_e$ and $\bar{\sigma}_m$) and the "local stress" (which is the averaged equivalent stress of the matrix, $\bar{\sigma}_{e0}$) under any external load. When there is no interface residual stress, i.e. $\tau_0 = 0$, Eq. (36) reduces to that of Chen et al. (2008a) without micropolar.

During uniaxial loading, the macroscopic applied stress $\bar{\sigma}$ equals to the macroscopic Mises stress $\bar{\sigma}_e$, and $\bar{\sigma}_m = \bar{\sigma}/3$. Thus,

$$\bar{\sigma}^2\left[\left(\frac{\mu_0}{\overline{G}}\right)^2\frac{\partial\overline{G}}{\partial\mu_0} + \frac{1}{3}\left(\frac{\mu_0}{\overline{K}}\right)^2\frac{\partial\overline{K}}{\partial\mu_0}\right] - 6\bar{\sigma}\tau_0\mu_0^2\frac{\partial\overline{B}}{\partial\mu_0} + 3\frac{f_1}{V_1}\tau_0^2\mu_0^2\frac{\partial\overline{D}}{\partial\mu_0} = (1 - f)\bar{\sigma}_{e0}^2 \tag{37}$$

For linear elastic materials, Eq. (37) gives a direct relationship between the macroscopic stress and local stress. For nonlinear material, the moduli in Eq. (37) should be substituted by the instantaneous secant moduli of nonlinear material, which are functions of local stress. For the nanocomposite or nanoporous material, the secant moduli of metal matrix are assumed to depend only on the averaged von Mises stress $\bar{\sigma}_{e0}$. Specifically, for a nonlinear matrix material whose uniaxial stress–strain curve is $\sigma = \sigma(\varepsilon)$, the secant Young's modulus is

$$E_s = \frac{\sigma(\varepsilon)}{\varepsilon} = E_s(\sigma_e) \tag{38}$$

Since of the hydrostatic stress does not influence the plastic deformation of the metal matrix, we assume that the bulk modulus k_0 is constant and deformation-independent. The secant shear modulus and secant Poisson's ratio are, respectively:

$$\mu_{0s} = \frac{3k_0E_{0s}}{9k_0 - E_{0s}} \tag{39}$$

$$\nu_{0s} = \frac{3k_0 - E_{0s}}{6k_0} \tag{40}$$

In this paper, the secant moduli are denoted by subscript *s*.

2.6. Solution procedure

The overall nonlinear response of composite can be obtained from the linear comparison material, following the procedures: (i) Substituting $\bar{\sigma}_{e0}$ into Eqs. (38) and (39) to obtain the secant Young's modulus and secant shear modulus of the metal matrix. (ii) Substituting Eqs. (24)–(32) into Eqs. (36) and (37), where the moduli of matrix (e.g. ν_0) is replaced by its secant moduli (e.g. ν_{0s}). Thus, a nonlinear equation which correlates the macroscopic stress with $\bar{\sigma}_{e0}$ (of the linear comparison material) is obtained.

The conventional solution procedure (e.g. Qiu and Weng, 1992, 1995) is that for a given macroscopic stress $\bar{\boldsymbol{\sigma}}$, its equivalent part $\bar{\sigma}_e$ and hydrostatic part $\bar{\sigma}_m$ are first obtained and then substituted into Eq. (36), and iteration is required so as to solve the averaged (matrix) equivalent stress, $\bar{\sigma}_{e0}$. Such iteration procedure is often of low efficiency.

Since a $\bar{\sigma}_{e0}$ can be always solved for a given macroscopic stress $\bar{\boldsymbol{\sigma}}$, that means for a given $\bar{\sigma}_{e0}$ there may be a corresponding $\bar{\boldsymbol{\sigma}}$ (although sometimes, from a given $\bar{\sigma}_{e0}$ the solution of $\bar{\boldsymbol{\sigma}}$ may not exist). Thus, in Eq. (36) one may take $\bar{\sigma}_{e0}$ as "known", and then solve for $\bar{\sigma}_e$ and $\bar{\sigma}_m$ – any real solution could correlate $\bar{\sigma}_{e0}$ with $\bar{\boldsymbol{\sigma}}$, and such algorithm does not need any iteration.

The macroscopic strain $\bar{\boldsymbol{\varepsilon}}$ corresponding the reference configuration can be obtained from the macroscopic stress as follows. Substitute the secant moduli k_0 and μ_{0s} into the expression of $\overline{\mathbf{C}}$, and the macroscopic secant compliance $\mathbf{C}_\tau$ is obtained. Recall that,

$$\bar{\boldsymbol{\varepsilon}} = \bar{\boldsymbol{\varepsilon}}_\sigma + \bar{\boldsymbol{\varepsilon}}_\tau = \overline{\mathbf{C}} : \bar{\sigma} + \overline{\mathbf{B}}\tau_0 \tag{41}$$

Both macroscopic secant compliances, $\overline{\mathbf{C}}$ and $\overline{\mathbf{B}}$, depend on $\bar{\sigma}_{e0}$. In the initial configuration when there is no external load, due to the interface residual stress τ_0, the RVE has a residual strain $\bar{\boldsymbol{\varepsilon}}_0$ where $\bar{\boldsymbol{\varepsilon}}_0 = \overline{\mathbf{B}}_{0s}\tau_0$, with $\overline{\mathbf{B}}_{0s}$ the secant coupling compliance tensor of the matrix at the initial state. After the external load is applied, the real (measurable) macroscopic strain is the strain change from the initial configuration to the current configuration, as follows:

$$\bar{\boldsymbol{\varepsilon}}_{real} = \overline{\mathbf{C}} : \bar{\boldsymbol{\sigma}} + \left(\overline{\mathbf{B}} - \overline{\mathbf{B}}_{0s}\right)\tau_0 \tag{42}$$

The final results of strains presented in the next section are all with respect to $\bar{\boldsymbol{\varepsilon}}_{real}$ unless otherwise denoted. Eq. (42) shows that for nonlinear materials, the external load and the interface residual stress are coupled, in addition to the substitution of the moduli with secant moduli; for a linear elastic material, $\overline{\mathbf{B}} = \overline{\mathbf{B}}_{0s}$ and thus $\bar{\boldsymbol{\varepsilon}}_{real} = \overline{\mathbf{C}} : \bar{\boldsymbol{\sigma}}$.

By following the steps outlined above, the overall stress–strain relationship of the composite RVE is obtained. The interface has two main effects, the first one is that the interface residual stress contributes to the residual stress field in the RVE which leads to an asymmetric tension-compression plastic deformation, the other one is that the interface moduli changes the overall moduli of RVE. The results are discussed below for specific material examples. Although the formulation in this section is specified for the macroscopically isotropic materials with nano-inclusions, it can be extended to macroscopically anisotropic materials with different interface properties.

3. Results and discussion

3.1. Metal nanoporous materials

As an illustrative example, we analyze the effect of surface on the plasticity of nanoporous aluminum. From previous experimental and atomistic simulations, the effective parameters of the aluminum surface are determined. The surface residual stress is $\tau_0 = 1.25\ (J/m^2)$ (Cammarata, 1994). Two sets of surface parameters are used: type-A ([1, 0, 0] surface) with $k_s = -5.457$ N/m and $\mu_s = -6.2178$ N/m, and type-B ([1, 1, 1] surface) with $k_s = 12.932$ N/m and $\mu_s = -0.3755$ N/m (Miller and Shenoy, 2000; Sharma and Bhate, 2003). We remark that in general, these parameters depend on crystal orientation; in this paper we assume the surface properties are homogeneous and isotropic. Thus, these parameters only serve as the order-of-magnitude estimations that could illustrate the effects of surface stress.

The aluminum bulk material is assumed to satisfy the power law hardening rule:

$$\sigma = \begin{cases} E_\varepsilon, & \sigma \le \sigma_y \\ \sigma_y + \frac{\sigma_y}{E}\varepsilon^{\frac{1}{3}}, & \sigma > \sigma_y \end{cases} \tag{43}$$

The bulk parameters are $E = 68.5$ GPa and $\nu = 0.35$, with an initial yield strength $\sigma_y = 250$ MPa.

3.1.1. Overall trend of surface effect

We first investigate the variation of the uniaxial yield strength of the nanoporous solid with respect to different types of surface, inclusion radius (R), and inclusion volume fraction, shown in Fig. 2. Here, the classical (reference) result refers to that without the size effect (in the limit $R \to \infty$). The positive and negative yield strength curves represent that under tension and compression, respectively. With the assistance of surface stress, the uniaxial yield strength is size-dependent and tension-compression asymmetric. For both types of surfaces, the yield stress is smaller than that without the surface effect, and the yield stress also decreases with the increase of the volume fraction of voids. With the current sign of the surface stress, the tensile yield strength is higher than the magnitude of the compressive yield strength. However, the difference between type-A surface and type-B surface is relatively small at $R = 10$ nm (the difference is even smaller if a larger R value is taken), which indicates that the effect of surface elasticity is less prominent than the surface residual stress.

3.1.2. Effects of surface elasticity and surface residual stress on yield surface

Since the surface effect includes both the surface residual stress and surface elasticity, in order to clarify their different roles, we may decouple these two effects and first focus on the effect of surface elasticity, by temporarily neglecting the surface residual stress. In Fig. 3 the yield surface is given as a function of nanopore radius to show its size effect. For type-A surface (Fig. 3a), the surface elasticity decreases the yield surface as the radius of nanopore is reduced, and such effect is more obvious along the Mises stress axis (y-axis). For type-B surface, the surface elasticity enlarges the yield surface, especially along the hydrostatic stress axis (x-axis in Fig. 3b). The difference between Fig. 3a and b illustrates the different surface elasticity of type-A and type-B surfaces. It is important to note that for both surfaces, the effect of surface elasticity becomes prominent only when R is below about 10 nm; otherwise, the yield surface at larger R values is close to that of the reference yield surface without surface effect. Another significant phenomenon is that the effect of surface elasticity on the yield strength is symmetric with respect to tension and compression.

Next, the surface residual stress is taken into account along with surface elasticity. Fig. 4a shows the nanoporous material with type-A surface, where with the decrease of R, the yield surface shifts significantly along the hydrostatic stress axis. At the same time the shape of the yield surface also changes a little bit (similar to that in Fig. 3a). The yield surface shift is caused by the surface residual stress. The surface residual stress combining with the curvature of surface causes a normal traction force on the surface. With the decreases of radius of pores, the traction force becomes more and more significant, hence the size effect. In the current model, the effect of normal traction force of the spherical void surface on the plastic deformation of matrix can only be counterbalanced by a macroscopic hydrostatic load. That is the reason why the surface residual stress can shift the yield surface along the hydrostatic axis. Due to the surface residual stress, the yield surface is no longer symmetric about the Mises stress axis. For material with type-B surface, the trend of yield surface variation is similar (Fig. 4b). Since the residual stress is identical for these two types of surfaces, the shift of both yield surfaces is identical in Fig. 4a and b.

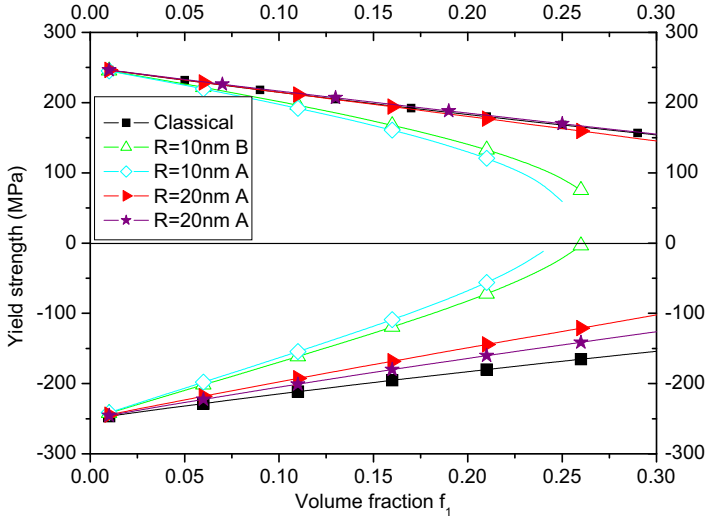

Fig. 2. Uniaxial tensile (positive) and compressive (negative) yield strengths of nanoporous aluminum, as a function of void volume fraction (f_1), void radius (R), and type of surface (A or B). In this paper, the classical result is a reference benchmark where there is no size effect ($R \to \infty$).

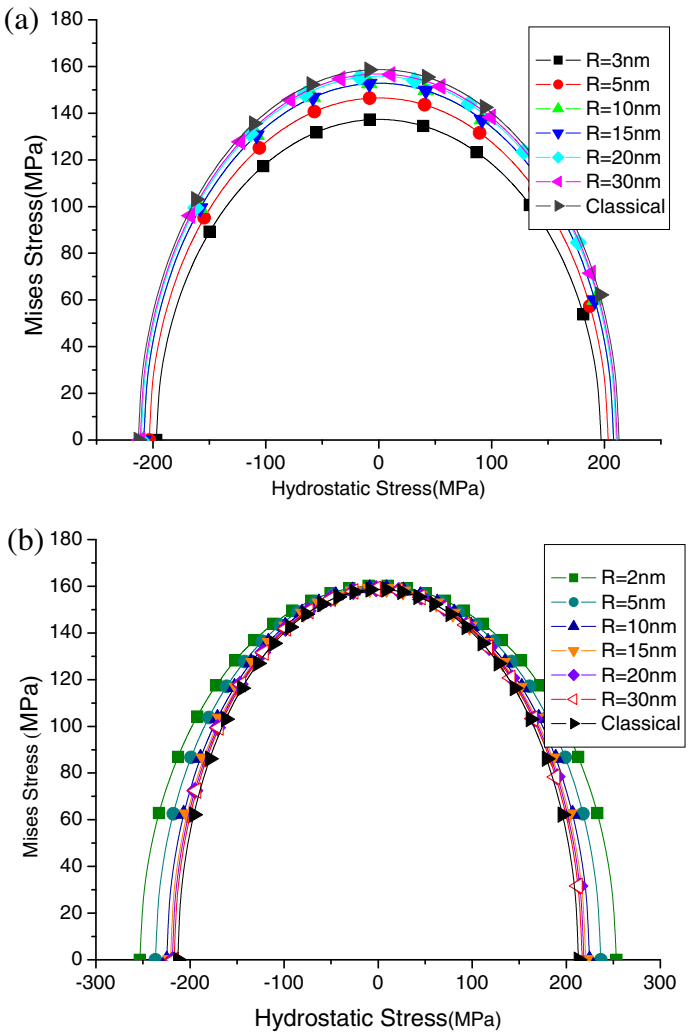

Fig. 3. Variation of the yield surface of nanoporous aluminum, as the pore size is varied with void volume fraction of 30%. Only the surface elasticity is taken into account. (a) Type-A surface and (b) type-B surface.

In a short summary, the surface elasticity and surface residual stress play very different roles affecting the yield surface of nanoporous materials. The surface elasticity can change the size and shape of yield surface, and its effect is tension-compression symmetric. By contrast, the surface residual stress may shift the yield surface along the hydrostatic stress axis, inducing asymmetry. It should be noted that such conclusion holds only for the isotropic matrix with spherical voids.

3.1.3. Size-dependent and asymmetric properties of tension and compression

The uniaxial yield strength of nanoporous materials is size-dependent as shown in Fig. 5, where the volume fraction of void is fixed at 30%. It is verified again that the effect of surface elasticity (i.e. the difference between type-A and type-B surfaces) is small, and the size effect is mainly due to the surface residual stress. The main reason for the dominance of surface residual stress is that the effect of surface elasticity comes through surface deformation, which is usually very small. In addition, the surface residual stress causes different effects on the yield strength upon tension and compression. With the reduced inclusion size, the magnitude of compressive yield strength decreases more quickly than that under tension. When the radius of nanovoid is sufficiently small, the yield strength may become 0, which means that the surface stress alone can cause the matrix to yield. When $R > 50$ nm, the result approaches to that of the reference solution with tension-compression symmetry, and that implies the surface stress effect is more prominent if the void radius is smaller than about 50 nm in the current example.

Now we consider the effect of surface stress on the overall stress–strain curves of the nanoporous material. It should be pointed out that the interface model of Eq. (2) is only valid for small deformation and the strain in Eq. (2) should be elastic (Vermaak et al., 1968). At the onset of yielding, the deformation of the surface is still small and elastic, and thus the surface

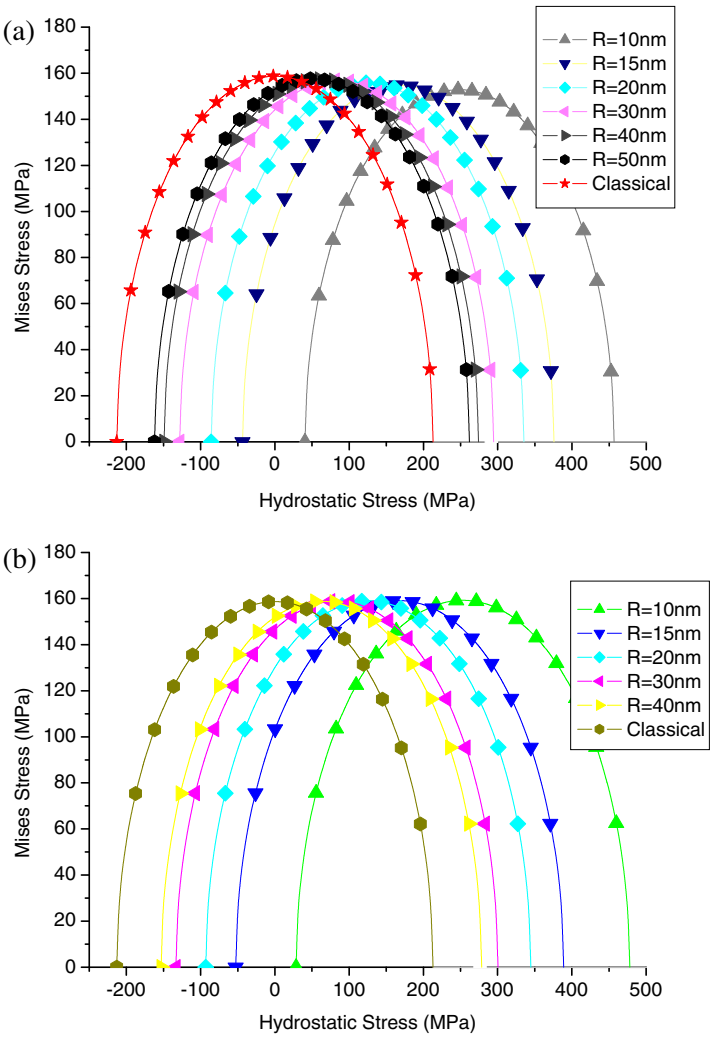

Fig. 4. Variation of the yield surface of nanoporous aluminum, as the pore size is varied with void volume fraction of 30%. Both surface elasticity and surface residual stress are taken into account. (a) Type-A surface and (b) type-B surface.

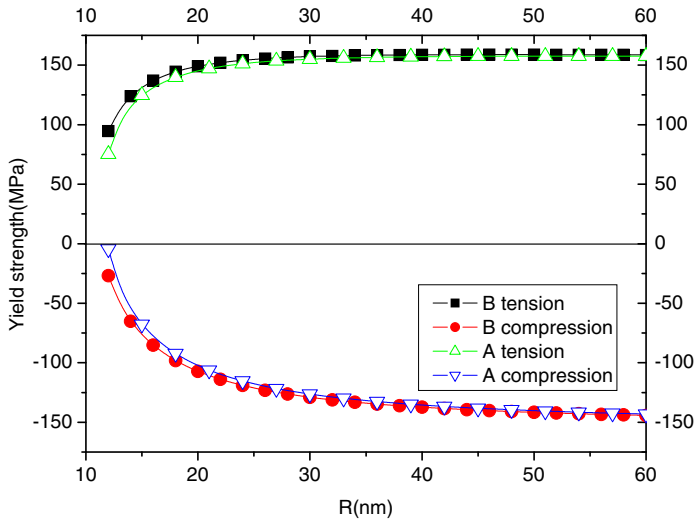

Fig. 5. The size-dependent compressive and tensile yield strength, for type-A and type-B surfaces (f_1 = 30%).

elasticity term must be considered when studying the yield strength of nanoporous materials. When the overall deformation is finite and plastic, since the surface energy γ is almost invariant with strain, the contribution of surface elasticity is small (with respect to Eqs. (1) and (2)). In addition, previous analyses have already shown that the effect of surface elasticity is small compared with that of surface residual stress, thus, we may neglect the surface elasticity when studying the whole uniaxial stress–strain curves of the nanoporous solid.

Fig. 6 shows the stress–strain curves of the nanoporous aluminum. With the decrease of void radius, plastic flow becomes easier, and the elastic deformation range is smaller and smaller. When R is smaller than about 10 nm, a small external load can cause plastic deformation, whereas when R is larger than about 50 nm, the effect of surface on the overall stress–strain curve of the nanoporous solid becomes negligible.

One may define a nominal Poisson's ratio, as the negative ratio between the transverse strain and the axial strain during deformation (even when the deformation is plastic). From the results in Fig. 7, the surface stress has a significant influence on the nominal Poisson's ratio. Contrary to the classical porous material model, with the surface/size effect, the nominal Poisson's ratio is tension-compression asymmetric. And the surface stress causes the nominal Poisson's ratio to decrease upon compression and to increase when stretched.

3.2. Nanocomposites with metal matrix and hard nanoparticle inclusions

To study the effect of interface stress, we focus our attention on a metal matrix composite (MMC), the SiC nanoparticle reinforced aluminum matrix. This MMC is widely used in industry and many researchers reported the size effect of MMC

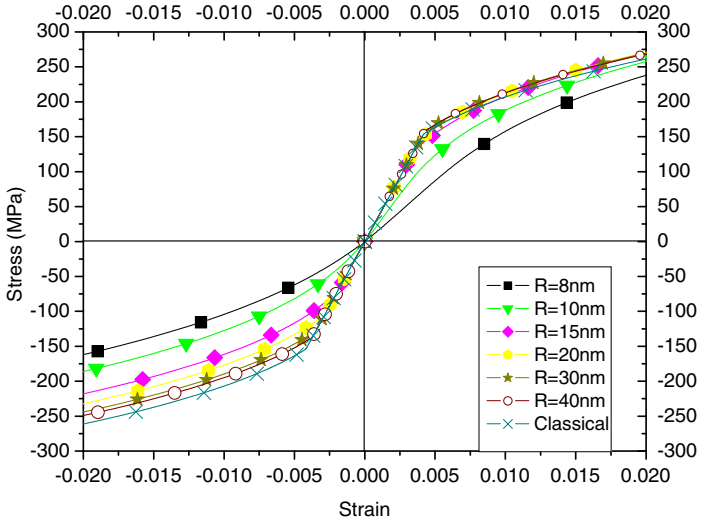

Fig. 6. Uniaxial stress–strain curves of nanoporous aluminum (f_1 = 30%) with varying pore sizes. The surface elasticity effect is ignored.

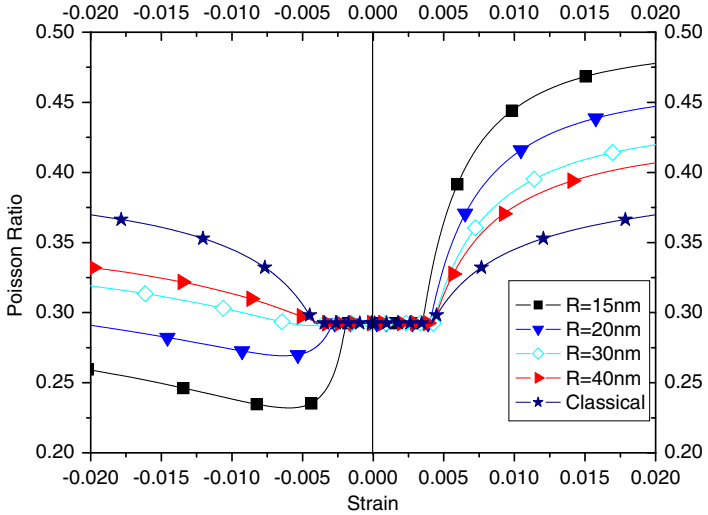

Fig. 7. The effect of surface residual stress on the nominal Poisson's ratio of nanoporous aluminum, as the pore radius is varied (f_1 = 30%).

when the inclusion size falls below several microns, and such an effect was explained by the strain gradient plasticity (Xue et al., 2001). Here we assume that the matrix and the particles are perfect bonded and there is no separation and slip during plastic deformation. When the particle size further decreases into nanoscale, the interface effect needs to be taken into account owing to the increased surface to volume ratio. Due of the lack of interface parameters, we continue to use the same surface parameters mentioned in the last section (for both types of interface), so as to gain some useful qualitative insights. The Young's modulus of the hard SiC particle is 250 GPa, and its Poisson's ratio is 0.25; the nanoparticle deforms elastically. During the whole deformation process, there is no debonding at the interface. The deformation of interface is also elastic since the nanoparticle is elastic. Both the interface residual stress and the interface elasticity are considered.

The effect of interface stress is coupled with particle volume fraction. For a given particle size, the more particle volume fraction, the larger the interface area and thus lead to a more significant effect, which are shown in Fig. 8a and b for tensile and compressive yield strengths, respectively. With the increase of f_1, the yield strength of the nanocomposite is significantly increased. Consistent with previous results, with the surface effect the yield strength is smaller than that without (i.e. classical), and the surface effect is more prominent as R reduces – this is due to the fact that the interface area is larger at smaller R (when the inclusion volume fraction is fixed). The effect of interface elasticity (difference between two types of surfaces) can be neglected, which is because of the deformation around hard particle is very small (much smaller than that around the nanopores in Section 3.1, and thus the contribution of interface elasticity is even smaller). Therefore, the size dependence of the yield strength of the RVE mainly comes from the interface residual stress. Comparison between Fig. 8a and b also reveals the tension-compression asymmetry, and the size effect of yield strength of the nanocomposite is more prominent upon tension.

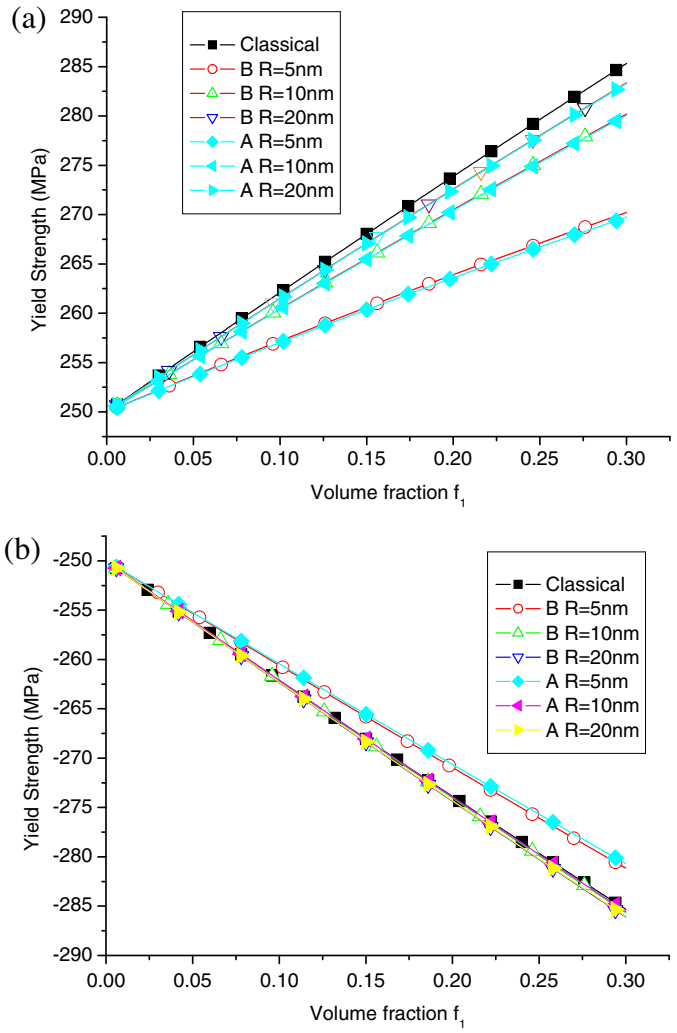

Fig. 8. The yield strength of SiC nanoparticle–Al matrix nanocomposite, as the inclusion volume fraction f_1 and radius R are varied, and for type-A and type-B surfaces. (a) Tensile strength and (b) compressive strength.

The uniaxial yield strength is size-dependent due to the effect of interface stress, as shown in Fig. 9 when f_1 is fixed at 30%. The radius of particle varies from 3 to 50 nm. Due to the interface stress (in particular the sign of the present interface residual stress), the tensile yield strength decreases with the decrease of particle radius. The effect of interface stress on the compressive yield strength is not monotonic: with the decrease of R, its magnitude first increases slightly and then decreases. Again, the effect of interface elasticity is very small and can be neglected even for very small hard inclusions.

Why is the effect of interface stress on the compressive yield strength not monotonic? The reason can be found by exploring the yield surface, Fig. 10, where $f_1 = 30\%$. The effect of interface elasticity is almost none and thus all influences come from the interface residual stress. The interface residual stress shifts the yield surface along the negative direction of the hydrostatic stress axis and the shape is basically unchanged. Whether the compressive yield strength is increased or decreased by the interface stress should depend on such shift amount. Note that on Fig. 10, the loading path of uniaxial compression can be represented by a straight line with slope (ratio between Mises and hydrostatic stresses) of -3. Thus, when the shift of yield surface is very small, the compressive yield strength increases slightly; when the shift amount is very large, the compressive strength decreases. However, regardless of the shift amount, the tensile yield strength always decreases. By comparing Fig. 10 with Fig. 4b, it can be seen that the effect of interface stress on the shifting of yield surface is opposite, for the cases of hard particle reinforced nanocomposite and nanoporous solid.

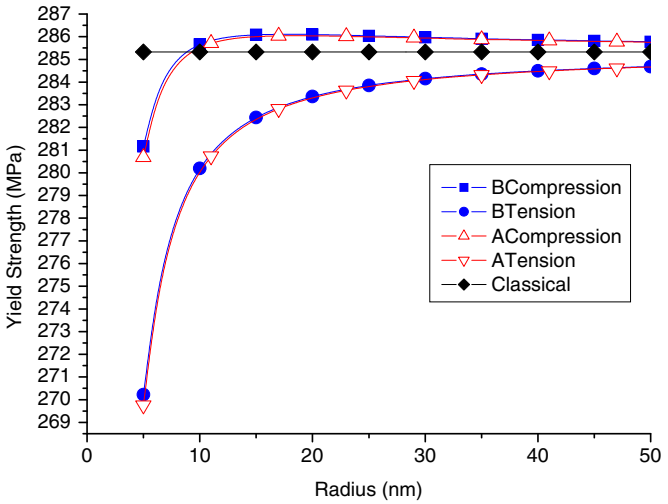

Fig. 9. The size-dependent yield strength of SiC nanoparticle reinforced Al nanocomposite ($f_1 = 30\%$). Both tensile strength and magnitude of compressive strength are shown, for type-B or type-A surfaces.

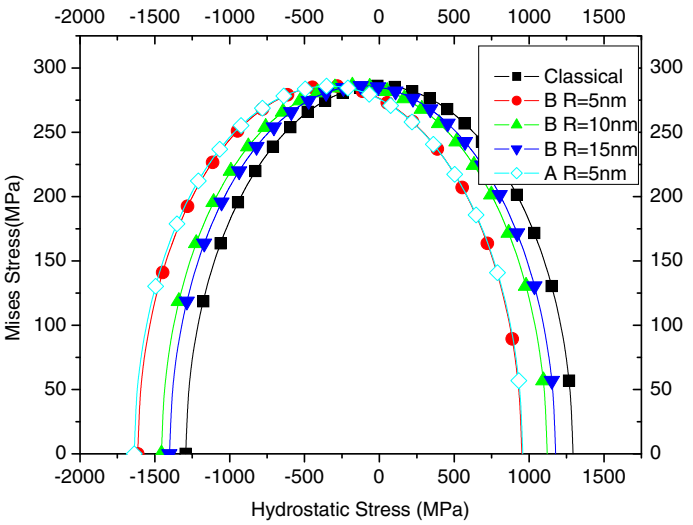

Fig. 10. The effect of interface stress on the yield surface of SiC nanoparticle reinforced Al composite ($f_1 = 30\%$). Both surface type and R are varied.

The uniaxial stress–strain curves are shown in Fig. 11 (with f_1 = 50%), from which the effect of interface stress is found to be relatively small for hard particle reinforced composites, even when the particle size is as small as 3 nm. Note that the scales used in the plots in Figs. 8 and 9 are different than that used in Fig. 11. The effect of interface stress is mainly reflected along the hydrostatic direction (Fig. 10), and the deformation of the interface between hard particle and matrix is much smaller than the free surface of a nanoporous material. Therefore, the effect of interface stress on plasticity of MMC is smaller than the surface effect on nanoporous metal. When the inclusion becomes softer, the stress concentration around the inclusion could cause a larger local deformation to enhance the effect of interface stress.

The interface stress can also make the nominal Poisson's ratio to decrease during tension and increase during compression (comparing with the classical results without interface stress), as shown in Fig. 12. However, such effect is also relatively small due to the aforementioned reasons.

For the nanocomposites studied in the present paper, the effect of interface energy becomes important when the size of nanoparticle inclusion is below several tens of nanometers. In other words, if in a hard particle reinforced MMC the size of particle is on the order of microns, the influence of interface is negligible. In this case, the size effect induced by micron-sized hard particles (e.g. the size effect of SiC reinforced MMCs reported by Lloyd (1994)) should not be attributed to the interface energy, instead it can be well explained by the strain gradient plasticity (Huang et al., 2004).

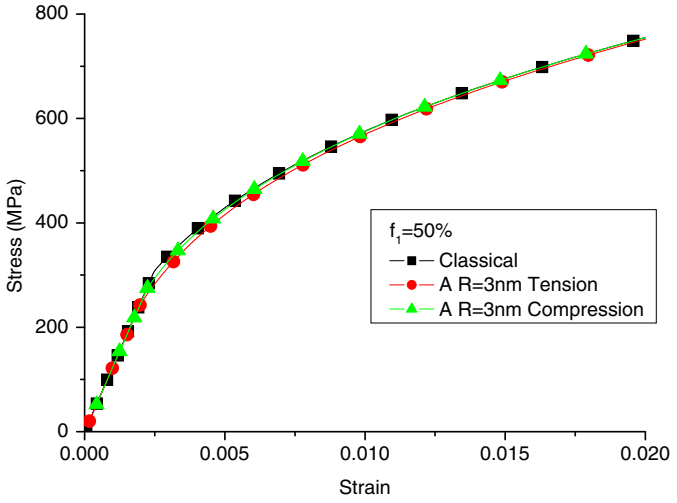

Fig. 11. Uniaxial stress–strain curves of SiC nanoparticle reinforced Al composite (f_1 = 50%); for the compression curve the magnitude of stress is shown. Only the results of R = 3 nm are given because at the plotted stress scale, the curves are close to each other when other inclusion sizes are used. The effect of surface elasticity is small and thus only the result of type-A surface is shown.

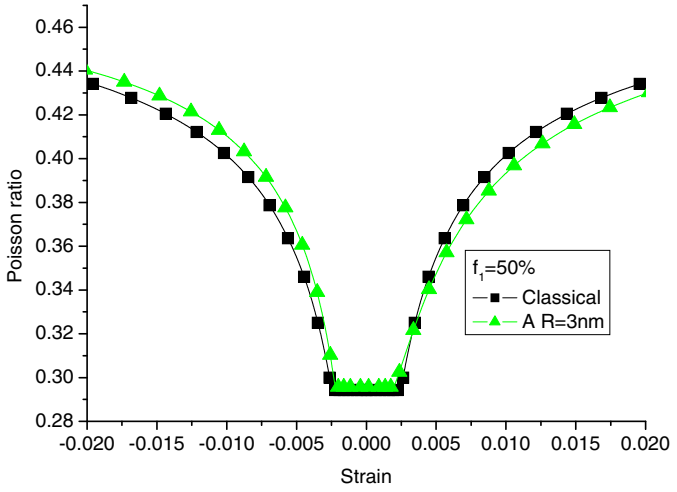

Fig. 12. Variation of the nominal Poisson's ratio of SiC nanoparticle reinforced Al composite (f_1 = 50%), with R = 3 nm. The effect of surface elasticity is small and thus only the result of type-A surface is shown.

3.3. Applying the continuum theory at the nanoscale

The present nonlinear micromechanics theory is based on continuum mechanics, yet we have attempted to apply the theory to explore the effect of surface/interface stress on the plastic deformation of nanoporous materials and nanocomposites. At the nanometer scale, the deformation is discrete and the application of continuum theory at this level is still controversial.

For metals, some researchers argued that at the nanometer scale, the deformation is characterized by discrete dislocation, which cannot be homogenized and represented by a continuum plasticity theory (Huang et al., 2004). Several discrete dislocation plasticity models have been suggested (Balint et al., 2008; Needleman and Van der Giessen, 2001b). It is true that when we study the local deformation characteristics (at the nanometer resolution), the discrete theory as well as molecular dynamics simulation (Potirniche et al., 2006) can obtain accurate results and reveal the nanoscopic deformation mechanism. However, during practical application, in many cases only the overall macroscopic mechanical behavior is important (and discrete dislocation and molecular dynamics simulations may be expensive). When we explore the overall response of heterogeneous materials (including the nanoporous and nanocomposite materials studied herein), the macroscopic mechanical behaviors are indeed the statistic average of the local deformation characteristics. For that matter, the micromechanics approach adopted in the present study is still plausible because it mainly concerns with the statistical average of the microscopic deformation, instead of pursuing the accurate high-resolution information of the local deformation (which is unnecessary in this case). In the current paper, the matrix around the nano-inclusion is assumed to satisfy the continuum theory. The local deformation obtained by the present method should be regarded as the average deformation of the matrix around all inclusions. Although the true local deformation is discrete (governed by dislocations), the statistic average of all local deformation can still be modeled as continuum.

Another important note is that the present paper is not limited to metals. The present theory can be applied to polymer materials whose deformation is not controlled by dislocation. Of course, there is no doubt that future investigations need to be carried out to clarify the link between the nanoscale deformation and the macroscopic response, and the micromechanics theory needs to be improved such that it is based more on deformation mechanisms.

The present study concerns with nanometer sized inclusions/voids, and we have shown that the surface/interface stress can cause the size effect of macroscopic plastic behaviors. Note that the size-dependent mechanical properties of materials may be originated from multiple factors, and another well-known cause is due to the strain gradient plasticity. The strain gradient effect is important for metal plasticity at the micron/sub-micron scale (Huang et al., 2004). Our investigation shows that the effect of interface energy of hard particle-reinforced MMC is relative small until the characteristic length scale is below several tens of nanometers. However, it still remains unclear whether there is an overlap between the effects of surface/interface energy and strain gradient. And further studies are needed to identify the transition from the nanoscale interface stress effect to microscale strain gradient effect.[4]

4. Concluding remarks

In this paper, we establish a new micromechanical framework to investigate the effect of interface stress on the plastic deformation of materials with nanosized inclusions. Both the interface residual stress and interface elasticity are considered. The theoretical approach is based on the second-order stress moment and the field fluctuation method of the secant moduli of nonlinear materials. The nonlinear coupling between the interface stress and external load is incorporated, and the results are simplified for a macroscopically isotropic RVE.

The interface stress causes size-dependency of the plastic properties of nanostructured materials, as well as tension-compression asymmetry – such contribution comes mainly from the interface residual stress instead of interface elasticity. In general, the interface/surface stress starts to affect the overall macroscopic mechanical behavior of the nanocomposite/nanoporous material if the characteristic particle/void size is below several tens of nanometers.

For nanoporous materials, the surface residual stress has a significant effect on the plastic deformation. It shifts the yield surface along the hydrostatic stress axis but does not change the shape and size of yield surface. The effect of surface elasticity on the plastic behavior is small, and it only changes the shape and size of yield surface slightly. With the surface effect, the variation of yield strength is more prominent with smaller nanopore size and higher pore volume fraction. With the present surface/material parameters of a nanoporous aluminum, the effect of surface elasticity starts to kick in only when the nanopore is smaller than about 10 nm, whereas the effect of surface residual stress becomes noticeable when the pore is smaller than about 50 nm. If the nanopore is small, the large surface effect could yield the overall material at very low external load, and below a critical size the nanoporous material yields under surface residual stress itself. There is a strong asymmetric behavior of the yield strength upon tension and compression, in terms of the yield stress, uniaxial stress–strain curve, and nominal Poisson's ratio.

For hard particle reinforced nanocomposite, since the deformation of interface is very small, the effect of interface elasticity is even smaller than that of the nanoporous material, and such effect can be neglected even for very small inclusions.

[4] Another reason for not considering the strain gradient effect in the present paper is because our micromechanics approach can be applied to polymer materials, for which the validity of strain gradient plasticity is controversial. At this moment, there is no unified theory that could incorporate all relevant size effects (e.g. surface/interface stress effect and strain gradient effect) across multiple scales. The relevant fundamental exploration, from theoretical, numerical, and experimental aspects, needs to be implemented in future.

For the same reason, the effect of interface residual stress on the overall plasticity is also not very significant (comparing with the nanoporous material counterpart), except the shift of yield surface along the hydrostatic axis. It is expected that if the nano-inclusion is softer (more compliant), the effect of interface will become more prominent.

The theoretical framework established in this paper is versatile and can be extended to anisotropic material properties and heterogeneous inclusions. The results will be compared with available experiments in future. It is expected that the micromechanics model is useful for the evaluation of mechanical reliability of nanostructured materials.

Acknowledgments

W.X.Z. and T.J.W. are supported by the State 973 Program of China (2007CB707702) and NSFC (10902081). W.X.Z. is also supported by China Scholarship Council. X.C. is supported by National Science Foundation CMMI-CAREER-0643726, by National Natural Science Foundation of China (50928601), and by a WCU (World Class University) program through the National Research Foundation of Korea funded by the Ministry of Education, Science and Technology of Korea (R32-2008-000-20042-0). W.X.Z. thanks Jie Yin (Columbia University) for his assistance in proving the Hill's lemma.

Appendix A. Proof of the Hill's lemma for RVE with interface stress

From Eq. (12), we can obtain the Hill's condition of material with interface stress as following:

$$\langle \boldsymbol{\sigma} : \boldsymbol{\varepsilon} \rangle = \bar{\boldsymbol{\sigma}} : \bar{\boldsymbol{\varepsilon}} - \frac{f_i}{V_i} \int_{\partial V_i} \mathbf{n} \cdot [\boldsymbol{\sigma}] \cdot \mathbf{u}\, ds = \bar{\boldsymbol{\sigma}} : \bar{\boldsymbol{\varepsilon}} - \frac{f_i}{V_i} \int_{\partial V_i} \mathbf{n} \cdot [\boldsymbol{\sigma}] \cdot (\mathbf{I} - \mathbf{n} \otimes \mathbf{n} + \mathbf{n} \otimes \mathbf{n}) \cdot \mathbf{n}\, ds = \bar{\boldsymbol{\sigma}} : \bar{\boldsymbol{\varepsilon}} - \frac{f_i}{V_i} \mathbf{n} \cdot [\boldsymbol{\sigma}] \cdot \mathbf{P} \cdot \mathbf{u} + \mathbf{n} \cdot [\boldsymbol{\sigma}] \mathbf{n} u_n\, ds \tag{A.1}$$

where $u_n = \mathbf{n} \cdot \mathbf{n}$ is the normal displacement at the interface. By utilizing the equilibrium equation of interface (Eq. (8)):

$$\begin{aligned} \langle \boldsymbol{\sigma} : \boldsymbol{\varepsilon} \rangle &= \bar{\boldsymbol{\sigma}} : \bar{\boldsymbol{\varepsilon}} - \frac{f_i}{V_i} \int_{\partial V_i} (-\nabla_s \cdot \boldsymbol{\tau}) \cdot \mathbf{u} + (-\boldsymbol{\tau} : \mathbf{b}) u_n\, ds \\ &= \bar{\boldsymbol{\sigma}} : \bar{\boldsymbol{\varepsilon}} - \frac{f_i}{V_i} \int_{\partial V_i} -\nabla_s \cdot (\boldsymbol{\tau} \cdot \mathbf{u}) + \boldsymbol{\tau} : \nabla_s (\mathbf{u}_t + u_n \mathbf{n}) + (-\boldsymbol{\tau} : \mathbf{b}) u_n\, ds \\ &= \bar{\boldsymbol{\sigma}} : \bar{\boldsymbol{\varepsilon}} - \frac{f_i}{V_i} \int_{\partial V_i} -\nabla_s \cdot (\boldsymbol{\tau} \cdot \mathbf{u}) + \boldsymbol{\tau} : \boldsymbol{\varepsilon}_s + \boldsymbol{\tau} \cdot \mathbf{n} \cdot \nabla_s u_n + \boldsymbol{\tau} : u_n \nabla_s \mathbf{n} + (-\boldsymbol{\tau} : \mathbf{b}) u_n\, ds \end{aligned} \tag{A.2}$$

where $\nabla_s \mathbf{n} = \mathbf{b}$ and $\boldsymbol{\tau} \cdot \mathbf{n} = 0$. Thus,

$$\langle \boldsymbol{\sigma} : \boldsymbol{\varepsilon} \rangle = \bar{\boldsymbol{\sigma}} : \bar{\boldsymbol{\varepsilon}} - \frac{f_i}{V_i} \int_{\partial V_i} \boldsymbol{\tau} : \boldsymbol{\varepsilon}_{\mathbf{s}}\, ds + \frac{f_i}{V_i} \int_{\partial V_i} \nabla_s \cdot (\boldsymbol{\tau} \cdot \mathbf{u})\, ds \tag{A.3}$$

In several earlier works, the last term in Eq. (A.3) was directly assumed to be zero. However, this is not so straightforward. Now we prove that the last term in Eq. (A.3) equals to 0. The surface divergence follows the generalized Gauss theorem (Yin, 2005):

$$\int_S \nabla_s \cdot \mathbf{T}\, ds = \oint_{\partial S} \mathbf{m} \cdot \mathbf{T}\, dl - \int_S 2H \mathbf{n} \cdot \mathbf{T}\, ds \tag{A.4}$$

where $\mathbf{T}$ is an arbitrary continuous vector field, H is the mean curvature and $\mathbf{m}$ is the unit normal vector of the boundary curve which is in the tangent plane of the surface. For a closed surface, the first term of the right side of Eq. (A.4) is zero. From the above equation,

$$\int_{\partial V_i} \nabla_s \cdot (\boldsymbol{\tau} \cdot \mathbf{u})\, ds = -\int_{\partial V_i} 2H \mathbf{n} \cdot (\boldsymbol{\tau} \cdot \mathbf{u})\, ds = 0 \tag{A.5}$$

Thus,

$$\bar{\boldsymbol{\sigma}} : \bar{\boldsymbol{\varepsilon}} - \frac{f_i}{V_i} \int_{\partial V_i} \boldsymbol{\tau} : \boldsymbol{\varepsilon}_s\, ds = \langle \boldsymbol{\sigma} : \boldsymbol{\varepsilon} \rangle \tag{A.6}$$

Which is Eq. (13) in the text.

Appendix B. Derivation of the macroscopic moduli

The tensor $\overline{\mathbf{B}}$ and scale $\overline{D}$ can be derived from the Hashin sphere model (Hashin and Shtrikman, 1963). Each composite sphere (with radius r_2) consists of a spherical core (of radius r_1, which equals to R) that is surrounded by a matrix shell whose outer radius is r_2. Between the matrix and the inclusion there is an interface stress. The volume fraction of the core in the composite sphere is identical to the volume fraction of the inclusion in the real composite, i.e. $f_1 = (r_1/r_2)^3$. Thus, the real

composite material can be modeled by filling the composite space by the sphere model (the size of the spheres may be different but the configuration is the same). Hence, the effective composite properties can be obtained by analyzing the sphere model. When there is an interface stress $\boldsymbol{\tau} = \tau \mathbf{I}^{(2)}$, the sphere will expand in an isotropic manner.

The displacement of the inner sphere (spherical core) is

$$u_r^1 = ar \tag{B.1}$$

where a is an undetermined constant related to interface stress $\boldsymbol{\tau}$. The displacement of the outer shell is

$$u_r^2 = br + \frac{c}{r^2} \tag{B.2}$$

Where b and c are also undetermined constants related to $\boldsymbol{\tau}$, and they also need to satisfy the traction-free boundary condition on the outer surface. The strain components are

$$\varepsilon_{rr} = \frac{u_r}{r} \tag{B.3}$$

At the interface the displacement is continuous and the stress jump is equal to $2\tau/R$, i.e.

$$u_r^1(r_1) = u_r^2(r_1), \sigma_{rr}^2(r_1) - \sigma_{rr}^1(r_1) = 2\tau/R \tag{B.4}$$

$$\tau = \tau_0 + k_s \varepsilon_{rr} \tag{B.5}$$

The macroscopic strain caused by $\boldsymbol{\tau}$ is $\bar{\varepsilon}_{rr} = u_r^2(r_2)/r_2$. For the spherical core, the strain by $\boldsymbol{\tau}$ is $\varepsilon_{rr1} = u_r^1(r_1)/r_1$. Utilizing the constitutive equations and boundary conditions, the strains $\bar{\varepsilon}_{rr}$ and ε_{rr1} can be obtained by solving Eqs. (B.1)–(B.5). Note that $\bar{\varepsilon}_{rr}$ and ε_{rr1} are functions of the interface stress, and thus they depend on the interface residual stress τ_0. With $\bar{\boldsymbol{\varepsilon}}_\tau = \bar{\varepsilon}_{rr}\mathbf{I}^{(3)}$ we can obtain $\overline{\mathbf{B}}$:

$$\overline{\mathbf{B}} = \overline{B}\mathbf{I}^{(3)} = \frac{2f_1(4\mu_0 + 3k_0)\mathbf{I}^{(3)}}{R\left[\mu_0(f_1 - 1)k_0 - \left(\frac{4}{3}f_1\mu_0 + k_0\right)\left(\frac{1}{2}\mu_0 k_s^r - \frac{3}{4}k_1\right)\right]} \tag{B.6}$$

From $\mathrm{tr}(\boldsymbol{\varepsilon}^s) = 2\varepsilon_{rr1}, \overline{D}$ can be obtained:

$$\overline{D} = \frac{(4\mu_0 f_1 + 3k_0)}{R^2\left[\mu_0(f_1 - 1)k_0 - \left(\frac{4}{3}f_1\mu_0 + k_0\right)\left(12\mu_0 k_s^r - \frac{3}{4}k_1\right)\right]} \tag{B.7}$$

They correspond to Eqs. (24) and (25) in the text.

References

Aifantis, K.E., Willis, J.R., 2005. The role of interfaces in enhancing the yield strength of composites and polycrystals. Journal of the Mechanics and Physics of Solids 53 (5), 1047–1070.

Balazs, A.C., Emrick, T., Russell, T.P., 2006. Nanoparticle polymer composites: where two small worlds meet. Science 314 (5802), 1107–1110.

Balint, D.S., Deshpande, V.S., Needleman, A., Van der Giessen, E., 2008. Discrete dislocation plasticity analysis of the grain size dependence of the flow strength of polycrystals. International Journal of Plasticity 24 (12), 2149–2172.

Banhart, J., 2001. Manufacture, characterisation and application of cellular metals and metal foams. Progress in Materials Science 46, 559–632.

Cammarata, R.C., 1994. Surface and interface stress effects in thin films. Progress in Surface Science 46, 1–38.

Cao, G., Chen, X., 2007. An energy analysis of size-dependent elastic properties of ZnO nanofilms. Physical Review B 76, 165407.

Cao, G., Chen, X., 2008. The size dependence and orientation dependence of elastic properties of ZnO films. International Journal of Solids and Structures 45, 1730–1753.

Chen, T., Dvorak, G.J., Benveniste, Y., 1992. Mori–Tanaka estimates of the overall elastic moduli of certain composite materials. ASME Journal Applied Mechanics 59 (3), 539–546.

Chen, X., Surani, F.B., Kong, X., Punyamurtula, V.K., Qiao, Y., 2006. Energy absorption performance of a steel tube enhanced by a nanoporous material functionalized liquid. Applied Physics Letters 89, 241918.

Chen, H., Liu, X.N., Hu, G., 2008a. Overall plasticity of micropolar composites with interface effect. Mechanics of Materials 40 (9), 721–728.

Chen, X., Cao, G., Han, A., Punyamurtula, V.K., Liu, L., Culligan, P.J., Kim, T., Qiao, Y., 2008b. Nanoscale fluid transport: size and rate effects. Nano Letters 8, 2988–2992.

Christensen, R.M., Lo, K.H., 1979. Solutions for effective shear properties in three phase sphere and cylinder models. Journal of the Mechanics and Physics of Solids 27, 315–330.

Diao, J., Gall, K., Dunn, M.L., 2004. Yield strength asymmetry in metal nanowires. Nano Letters 4, 1863–1867.

Dingreville, R., Qu, J., Cherkaoui, M., 2005. Surface free energy and its effect on the elastic behavior of nano-sized particles, wires and films. Journal of the Mechanics and Physics of Solids 53 (8), 1827–1854.

Duan, H.L., Wang, J., Huang, Z.P., Karihaloo, B.L., 2005. Size-dependent effective elastic constants of solids containing nano-inhomogeneities with interface stress. Journal of the Mechanics and Physics of Solids 53, 1574–1596.

Frogley, M.D., Ravich, D., Wagner, H.D., 2003. Mechanical properties of carbon nanoparticle-reinforced elastomers. Composites Science and Technology 63, 1647–1654.

Gall, K., Diao, J., Dunn, M.L., 2004. The strength of gold nanowires. Nano Letters 4, 2431–2436.

Gan, Y.X., Wei, C.-S.S., Lam, M., Wei, X., Lee, D., Kysar, J.W., Chen, X., 2007. Deformation and fracture behavior of electrocodeposited alumina nanoparticle/copper composite films. Journal of Materials Science 42, 5256–5263.

Gleiter, H., 2000. Nanostructured materials: basic concepts and microstructure. Acta Materialia 48, 1–29.

Gurtin, M.E., Murdoch, A.I., 1975. A continuum theory of elastic material surfaces. Archive for Rational Mechanics and Analysis 57, 291–323.

Hashin, Z., 1983. Analysis of composites: a survey. ASME Journal of Applied Mechanics 50, 481–505.

Hashin, Z., Shtrikman, S., 1963. A variational approach to the theory of the elastic behaviour of multiphase materials. Journal of the Mechanics and Physics of Solids 11, 127–140.

Hill, R., 1965. A self-consistent mechanics of composite materials. Journal of the Mechanics and Physics of Solids 13 (213-222).
Hu, G.K., 1996. A method of plasticity for general aligned spheroidal void or fiber reinforced composites. International Journal of Plasticity 12, 439–449.
Huang, Z.P., Wang, J., 2006. A theory of hyperelasticity of multi-phase media with surface/interface energy effect. Acta Mechanica 182 (3-4), 195–210.
Huang, Y., Qu, S., Hwang, K.C., Li, M., Gao, H., 2004. A conventional theory of mechanism-based strain gradient plasticity. International Journal of Plasticity 20 (4-5), 753–782.
Kitazono, K., Sato, E., Kuribayashi, K., 2003. Application of mean-field approximation to elastic-plastic behavior for closed-cell metal foams. Acta Materialia 51, 4823–4836.
Kornev, K.G., Sroloviz, D.J., 2004. Surface stress-driven instabilities of a free film. Applied Physics Letters 85, 2487.
Lee, Z., Ophus, C., Fischer, L.M., Nelson-Fitzpatrick, N., Westra, K.L., Evoy, S., Radmilovic, V., Dahmen, U., Mitlin, D., 2006. Metallic NEMS components fabricated from nanocomposite Al–Mo films. Nanotechnology 17, 3063–3070.
Li, L.X., Wang, T.J., 2005. A unified approach to predict overall properties of composite materials. Materials Characterization 54, 49–62.
Liu, L., Qiao, Y., Chen, X., 2008. Pressure-driven water infiltration into carbon nanotube: the effect of applied charges. Applied Physics Letters 92, 101927.
Liu, L., Chen, X., Lu, W., Qiao, Y., 2009. Infiltration of electrolytes into molecular-sized nanopores. Physical Review Letters 102, 184501.
Lloyd, D.J., 1994. Particle-reinforced aluminum and magnesium matrix composites. International Materials Reviews 39 (1), 1–23.
Lu, G.Q., Zhao, X.S., 2005. Nanoporous Materials: Science and Engineering, vol. 4. Imperial College Press.
Marszalek, P.E., Greenleaf, W.J., Li, H., Oberhauser, A.F., Fernandez, J.M., 2000. Atomic force microscopy captures quantized plastic deformation in gold nanowires. Proceedings of the National Academy of Sciences of the United States of America 97, 6282.
Miller, R.E., Shenoy, V.B., 2000. Size-dependent elastic properties of nanosized structural elements. Nanotechnology 11, 139.
Morris, R.E., Wheatley, P.S., 2008. Gas storage in nanoporous materials. Angewandte Chemie International Edition 47 (27), 4966–4981.
Moya, J.S., Lopez-Estebana, S., Pecharromán, C., 2007. The challenge of ceramic/metal microcomposites and nanocomposites. Progress in Materials Science 52, 1017–1090.
Needleman, A., Van der Giessen, E., 2001a. Discrete dislocation and continuum descriptions of plastic flow. Materials Science and Engineering A – Structural Materials Properties Microstructure and Processing 309, 1–13.
Needleman, A., Van der Giessen, E., 2001b. Discrete dislocation and continuum descriptions of plastic flow. Materials Science and Engineering A, 1–13.
Nemat-Nasser, S., Hori, M., 1993. Micromechanics: Overall Properties of Heterogeneous Materials. Elsevier, Amsterdam.
Nix, W.D., Gao, H., 1998. An atomistic interpretation of interface stress. Scripta Materialia 39 (12), 1653–1661.
Ou, Z.Y., Wang, G.F., Wang, T.J., 2008. Effect of residual surface tension on the stress concentration around a nanosized spheroidal cavity. International Journal of Engineering Science 46 (5), 475–485.
Ponte Castañeda, P., 1991. The effective mechanical properties of nonlinear isotropic composite. Journal of the Mechanics and Physics of Solids 39, 45–71.
Ponte Castañeda, P., 1996. Exact second-order estimates for the effective mechanical properties of nonlinear composite materials. Journal of the Mechanics and Physics of Solids 44 (6), 827–862.
Ponte Castañeda, P., Suquet, P., 1997. Nonlinear composites. Advances in Applied Mechanics 34, 171–302.
Potirniche, G.P., Horstemeyer, M.F., Wagner, G.J., Gullett, P.M., 2006. A molecular dynamics study of void growth and coalescence in single crystal nickel. International Journal of Plasticity 22 (2), 257–278.
Qiao, Y., Liu, L., Chen, X., 2009. Pressurized liquid in nanopores: a modified Laplace–Young equation. Nano Letters 9, 984–988.
Qiu, Y.P., Weng, G.J., 1992. A theory of plasticity for porous materials and particle-reinforced composites. ASME Journal of Applied Mechanics 59, 261–268.
Qiu, Y.P., Weng, G.J., 1993. Plastic potential and yield function of porous materials with aligned and randomly oriented spheroidal voids. International Journal of Plasticity 9, 271–290.
Qiu, Y.P., Weng, G.J., 1995. An energy approach to the plasticity of a two-phase composite containing aligned inclusions. ASME Journal of Applied Mechanics 62 (4), 1039–1046.
Russell, V.A., Evans, C.C., Li, W., Ward, M.D., 1997. Nanoporous molecular sandwiches: pillared two-dimensional hydrogen-bonded networks with adjustable porosity. Science 276 (5312), 575–579.
Sharma, P., Bhate, S.G.N., 2003. Effect of surfaces on the size-dependent elastic state of nano-inhomogeneities. Applied Physics Letters 82, 535.
Shuttleworth, R., 1950. The surface tension of solids. Proceedings of Physical Society of London A 63, 444–457.
Suquet, P., 1993. Overall potentials and extremal surfaces of power law or ideally plastic composites. Journal of the Mechanics and Physics of Solids 41, 981–1002.
Suquet, P., 1995. Overall properties of nonlinear composites: a modified secant moduli theory and its link with Ponte Castaneda's nonlinear variational procedure. Comptes Rendus de l'Academie des Sciences III (320), 563–571.
Tandon, G.P., Weng, G.J., 1988. A theory of particle reinforced plasticity. ASME Journal of Applied Mechanics 55, 126–135.
Teh, K.-S., Cheng, Y.-T., Lin, L., 2005. MEMS fabrication based on nickel-nanocomposite: film deposition and characterization. Journal of Micromechanics and Microengineering 15, 2205–2215.
Thostenson, E.T., Ren, Z., Chou, T.-W., 2001. Advances in the science and technology of carbon nanotubes and their composites: a review. Composites Science and Technology 61, 1899–1912.
Vermaak, J.S., Mays, C.W., Kuhlmann-Wilsdorf, D., 1968. On surface stress and surface tension – I. Theoretical considerations. Surface Science 12 (2), 128–133.
Wang, G.F., Feng, X.Q., 2007. Effect of surface elasticity and residual surface tension on the natural frequency of microbeams. Applied Physics Letters 90, 231904.
Wang, G.F., Wang, T.J., 2006a. Deformation around a nanosized elliptical hole with surface effect. Applied Physics Letters 89 (16).
Wang, G.F., Wang, T.J., 2006b. Deformation around a nanosized elliptical hole with surface effect. Applied Physics Letters 89, 161901.
Wang, G.F., Feng, X.Q., Wang, T.J., Gao, W., 2008. Surface effects on the near-tip stresses for mode-I and mode-III cracks. Journal of Applied Mechanics – Transactions of the ASME 75 (1).
Wu, B., Heidelberg, A., Boland, J.J., 2005. Mechanical properties of ultrahigh-strength gold nanowires. Nature Materials 4, 525–529.
Xue, Z., Huang, Y., Li, M., 2001. Particle size effect in metallic materials: a study by the theory of mechanism-based strain gradient plasticity. Acta Materialia 50 (1), 149–160.
Yang, F., 2006. Effect of interfacial stresses on the elastic behavior of nanocomposite materials. Journal of Applied Physics 99, 054306.
Yin, Y., 2005. Integral theorems based on a new gradient operator derived from biomembranes (part II): applications. Tsinghua Science and Technology 10 (3), 376–380.
Zhang, W., Wang, T.J., 2007. Effect of surface energy on the yield strength of nanoporous materials. Applied Physics Letters 90, 063104.
Zhang, W., Wang, T.J., Chen, X., 2008. Effect of surface stress on the asymmetric yield strength of nanowires. Journal of Applied Physics 103, 123527.
Zhang, W., Xu, Z., Wang, T.J., Chen, X., 2009. Effect of inner gas pressure on the elastoplastic behavior of closed-cell metal foams: a second-order moment micromechanics model. International Journal of Plasticity 25, 1231–1252.